

## 12

# Parahydrogen-Induced Polarization: Applications to Detect Intermediates of Catalytic Hydrogenations

Joachim Bargon

### 12.1

#### *In-Situ* Spectroscopy

The level of understanding the mechanisms of homogeneously catalyzed reactions correlates with information about reactive intermediates. Therefore, *in-situ* methods – that is, investigations based upon physical techniques conducted *during* the reactions – are highly desirable and important. For this purpose, a considerable scope of *in-situ* techniques based upon time-proven classical types of spectroscopy has been developed. Since many of the industrially important catalyzed reactions require the use of high pressures and high temperatures for optimum performance, ideally, these techniques should accommodate such conditions. Contemporary *in-situ* methods include specialized forms of optical or magnetic resonance spectroscopy, in particular vibration and rotation spectroscopy, such as infrared or Raman spectroscopy, or nuclear magnetic resonance (NMR) [1, 2]. This chapter will focus on the latter technique.

#### 12.1.1

##### *In-Situ* NMR Spectroscopy

For the elucidation of chemical reaction mechanisms, *in-situ* NMR spectroscopy is an established technique. For investigations at high pressure either sample tubes from sapphire [3] or metallic reactors [4] permitting high pressures and elevated temperatures are used. The latter represent autoclaves, typically machined from copper-beryllium or titanium-aluminum alloys. An earlier version thereof employs separate torus-shaped coils that are imbedded into these reactors permitting *in-situ* probing of the reactions within their interior. However, in this case certain drawbacks of this concept limit the filling factor of such NMR probes; consequently, their sensitivity is relatively low, and so is their resolution. As a superior alternative, the metallic reactor itself may function as the resonator of the NMR probe, in which case no additional coils are required. In this way gas/liquid reactions or reactions within supercritical fluids can be studied

conveniently at high pressure and elevated temperatures with much higher sensitivity [4].

### 12.1.2

#### ***In-Situ* PHIP-NMR Spectroscopy**

A number of years ago, an additional *in-situ* method to investigate hydrogenation reactions via NMR spectroscopy was introduced, which gives rise to a significant signal enhancement primarily of the proton NMR spectra; consequently, the intermediates and minor reaction products of homogeneous hydrogenations can be identified much more readily. This signal enhancement is due to proton spin polarization originally derived from separating the spin isomers of dihydrogen, which can readily be achieved at low temperatures. Using only one of these spin isomers for the hydrogenation – namely parahydrogen – NMR spectra recorded during homogeneous hydrogenations of various substrates in the presence of suitable organometallic catalysts exhibit considerable signal enhancement in the form of intense emission or absorption lines. In principle, either one of the two spin isomers – that is, ortho- or parahydrogen – may be used instead of ordinary dihydrogen ( $H_2$ ), though typically parahydrogen is employed. This phenomenon was originally observed experimentally by chance [5], but it has later been independently thought of theoretically, and has been attributed to symmetry breaking during the hydrogenation reaction [6].

This concept has originally been named PASADENA (Parahydrogen And Synthesis Allow Dramatically Enhanced Nuclear Alignment) [6], but the spectroscopic method based on this phenomenon has subsequently also been called PHIP (Para-Hydrogen Induced Polarization) [7]. In this chapter the abbreviation PHIP will be used throughout.

The signal enhancement due to this approach can, in principle, be as high as  $10^5$ -fold – that is, equal to the reciprocal Boltzmann factor; however, the experimentally achievable enhancement factors typically range between 10 and  $10^3$ . Thanks to this increase in sensitivity, the PHIP phenomenon, therefore, provides for a powerful tool to investigate the fate of the dihydrogen, the catalysts, and of the substrates during hydrogenation reactions.

The observed polarization is primarily associated with the former parahydrogen protons. However, other protons may also experience a drastic signal enhancement due to nuclear spin polarization transferred to these nuclei via the nuclear Overhauser effect (NOE) or similar processes, both in the final reaction products as well as in their precursor intermediates.

Likewise, the original proton polarization can be transferred to other magnetically active heteronuclei, notably to  $^{13}C$ ,  $^{15}N$ ,  $^{19}F$ ,  $^{29}Si$ ,  $^{31}P$  or appropriate isotopes of various transition metals. This is especially attractive because of the frequently low sensitivity of many heteronuclei, in particular of those with low magnetic moments [8].

Furthermore, in favorable cases, (para-)hydrogenation-derived spin polarization may be carried on to subsequent follow-up reactions, where it can serve to

boost the notoriously low sensitivity of NMR spectroscopy in general. For this purpose, the follow-up reactions have to be reasonably fast, such as the bromination of alkenes, for example [51].

The polarization patterns are dependent upon the strength of the magnetic field, in which the reactions are carried out. If the reactions are carried out at high fields (i.e., notably within the NMR spectrometer), the resonances appear in “antiphase” – that is, there is an equal number of absorption and emission lines and no net polarization. At low field however (i.e., when the reaction is carried out at zero or a very low field and then transferred into the high field of the NMR spectrometer for subsequent investigation), the resonances display net polarization, as has been outlined by Pravica and Weitekamp [9].

Initially in this chapter, the various features of the PHIP phenomenon, of the apparatus to enrich parahydrogen and orthodeuterium, and of the computer-based analysis or simulations of the PHIP spectra to be observed under specific assumptions will be outlined. In the following sections, comparisons of the experimentally obtained and of the simulated spectra reveal interesting details and mechanistic information about the hydrogenation reactions and their products.

## 12.2

### Ortho- and Parahydrogen

H<sub>2</sub> consists of two nuclear spin isomers, namely p-H<sub>2</sub> with antiparallel proton spins, and o-H<sub>2</sub> with parallel arrangement. Whereas p-H<sub>2</sub> is diamagnetic (i.e., it represents a singlet state (S)), o-H<sub>2</sub> shows nuclear paramagnetism with a resulting nuclear spin of one (Fig. 12.1). Its three allowed alignments relative to an external magnetic field – namely with, against, or orthogonal to the field – are labeled T<sub>+1</sub>, T<sub>-1</sub> or T<sub>0</sub>, respectively (Fig. 12.2). Accordingly, in the absence of a magnetic field, o-H<sub>2</sub> is degenerate threefold, and in thermal equilibrium at room temperature, n-H<sub>2</sub> consists of 25.1% p-H<sub>2</sub> and of 74.9% o-H<sub>2</sub>; that is, the ratio is approximately 1:3 [10].

Due to symmetry requirements, only specific quantum states of the spin and of the rotational states of H<sub>2</sub> are mutually compatible. Therefore, the energeti-

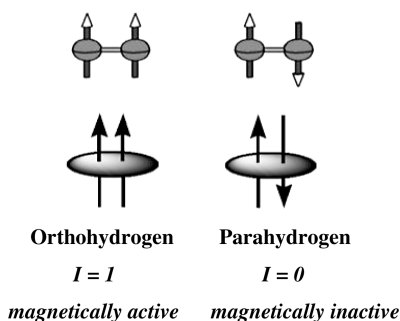


**Fig. 12.1** The spin isomers of molecular hydrogen (“dihydrogen”).

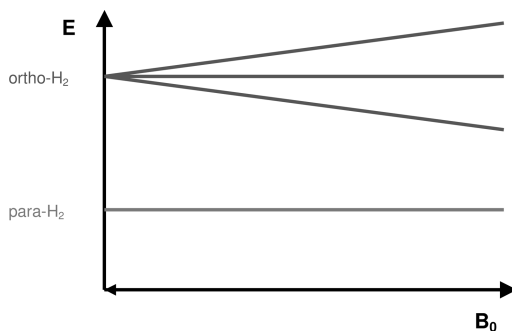


**Figure 12.2** Magnetic field dependence of the energy levels of ortho- and para- $\text{H}_2$ . Parahydrogen ( $\text{p-H}_2$ ) is a singlet that is unaffected by the magnetic field, whereas orthohydrogen ( $\text{o-H}_2$ ) is a triplet. Its energy levels split, showing the Zeeman effect.

cally lowest state of  $\text{H}_2$  corresponds to  $\text{p-H}_2$ , which prevails at cryogenic temperatures. This fact is used to enrich fractions in  $\text{p-H}_2$ . Even though both spin isomers,  $\text{p-H}_2$  and  $\text{o-H}_2$ , can even be separated completely, the  $\sim 50\%$  enrichment of  $\text{p-H}_2$  achieved at 77 K using liquid nitrogen as a coolant is sufficient for conducting parahydrogen labeling experiments [11].

### 12.2.1

#### Magnetic Field Dependence of the PHIP-Phenomenon: PASADENA and ALTADENA Conditions

According to Bowers and Weitekamp [6],  $^1\text{H}$  spin polarization occurs in the hydrogenation products of  $\text{p-H}_2$ , if a chemical reaction breaks its initial symmetry. Pure  $\text{p-H}_2$  itself is NMR-inactive (i.e., it cannot be detected via  $^1\text{H-NMR}$ ). Correspondingly, since hydrogenation of an asymmetrically substituted acetylene yields an olefin with chemically inequivalent protons, the use of  $\text{p-H}_2$  give rise to two resonances, typically consisting of doublets with one component in emission and one in absorption each (“antiphase doublets”) [6]. Bowers and Weitekamp named this phenomenon PASADENA, which applies to reactions carried out within the high magnetic field of a NMR spectrometer.

Figure 12.3 outlines the essential features of the PASADENA/PHIP concept for a two-spin system. If the symmetry of the  $\text{p-H}_2$  protons is broken, the reaction product exhibits a PHIP spectrum (Fig. 12.3, lower). If the reaction is carried out within the high magnetic field of the NMR spectrometer, the PHIP spectrum of the product consists of an alternating sequence of enhanced absorption and emission lines of equal intensity. This is also true for an AB spin system due to a compensating balance between the individual transition probabilities and the population rates of the corresponding energy levels under PHIP conditions. The NMR spectrum after the product has achieved thermal equilibrium exhibits intensities much lower than that of the intermediate PHIP spectrum.

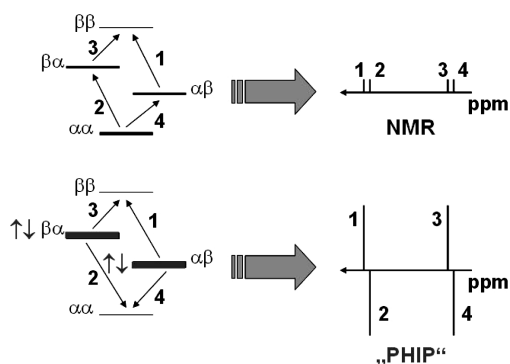


Fig. 12.3 Regular NMR (upper) and high-field PHIP-NMR spectrum (lower) of a two-spin AX system.

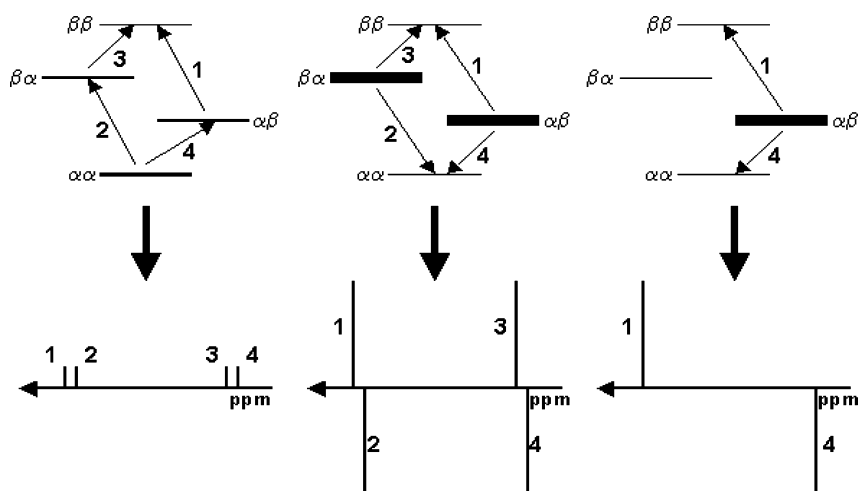


Fig. 12.4 Normal NMR, high-field (PASADENA) and low-field (ALTADENA) PHIP.

A related phenomenon occurs if the reactions are carried out at low field outside, but where the samples are transferred immediately thereafter into the spectrometer for subsequent NMR analysis. This variety has been termed ALTA-DENA (Adiabatic Longitudinal Transport After Dissociation Engenders Net Alignment) [9]. Other authors [7] have since used the acronym PHIP as an alternative for the same phenomenon.

An essential requirement for the occurrence of PHIP is that the rates of the reactions compete favorably with the relaxation of the nuclear spins in the products; therefore, the reaction rates must be faster than the relaxation rates, and the polarization must be detected during the reactions – that is, *in situ*.

Today, many examples have been reported which demonstrate the potential of the PHIP technique as a powerful analytical tool to investigate the reaction mechanisms of homogeneously catalyzed hydrogenations [12].

For more complex spin systems, a computer program PHIP<sup>+</sup> has been developed [13, 45] which allows the expected PHIP spectra to be calculated from the chemical shifts and coupling constants of the products. Depending upon which proton pair in the product molecule stems from p-H<sub>2</sub>, different – but characteristic – polarization patterns result [14]. The patterns also depend on the sign of the coupling constants. Simple “sign rules” governing the relative sequence of the emission and absorption lines in the PHIP spectra (i.e., their “phase”) can be formulated in similar manner to the “Kaptein Rules” of chemically induced dynamic nuclear polarization (CIDNP) [15].

### 12.2.2

#### PHIP, CIDNP, and Radical Mechanisms

In appearance, the PHIP phenomenon closely resembles those due to CIDNP [16], another phenomenon, which also gives rise to emission and enhanced absorption lines in NMR spectra. However, CIDNP is the consequence of the occurrence of free radicals, and previously has frequently been considered unequivocal proof for free radical reactions.

The fact that two entirely different phenomena can both yield nuclear spin polarization may cause confusion; therefore, the appearance of intense emission and absorption lines during *in-situ* NMR investigations of hydrogenation reactions is not necessarily proof for free radical intermediates, and examples of erroneous conclusions do exist [5].

For the mechanisms of homogeneous catalysis this may seem irrelevant, but as early as 1977 – long before the discovery of PHIP – Halpern [16e] had used “...the observation of CIDNP...” to “...establish a radical reaction path...” during the hydrogenation of styrene with an organometallic catalyst. Given the fact that even at room temperature (i.e., without any cooling of dihydrogen) there is a slight excess of parahydrogen, which is well capable of giving rise to “CIDNP-like phenomena” in the <sup>1</sup>H-NMR spectra, observations of emission and enhanced absorption lines alone are no longer a reliable proof of the occurrence of free radicals, if H<sub>2</sub> is involved. Therefore, caution is recommended, especially when exploiting the results of earlier investigations. Today, it is easy to err on the safe side, since a reliable discrimination exists between the alternatives CIDNP and PHIP, using both enriched ortho- and parahydrogen in independent runs [17]. In this way it should be possible to ascertain, whether a “...radical reaction pathway in homogeneous hydrogenation” [16e] really exists by using both para- and orthohydrogen in subsequent experiments.

## 12.2.3

**Preparation of Parahydrogen**

Molecular hydrogen or dihydrogen ( $H_2$ ) occurs in two isomeric forms, namely with its two proton spins aligned either parallel (ortho-hydrogen) or antiparallel (parahydrogen) (see Fig. 12.1). Parahydrogen was first prepared during the 1920s by Bonhoeffer and Harteck [18]. The separation of both spin isomers [10] has also been possible for many years, even though ortho-hydrogen – the energetically less favorable form – is occasionally still described in the literature as “obtainable only in theory” [20a], especially in older text books [20 b].

**12.2.3.1 Parahydrogen Enrichment**

As stated earlier, in the state of thermal equilibrium at room temperature, dihydrogen ( $H_2$ ) contains 25.1% parahydrogen (nuclear singlet state) and 74.9% ortho-hydrogen (nuclear triplet state) [19]. This behavior reflects the three-fold degeneracy of the triplet state and the almost equal population of the energy levels, as demanded by the Maxwell-Boltzmann distribution. At lower temperatures, different ratios prevail (Fig. 12.5) due to the different symmetry of the singlet and the triplet state [19].

Since interconversions between different states of symmetry (i.e., between ortho- and parahydrogen) are forbidden, the adjustment of the relative ratios of the two spin isomers to the values corresponding to the thermal equilibrium at an arbitrary temperature is normally very slow and, therefore, must be catalyzed. In the absence of a catalyst, dihydrogen samples retain their once achieved ratio and, accordingly, they can be stored in their enriched or separated forms for rather long periods (a few weeks or even a few years in favorable cases).

In spite of the fact that ortho- or parahydrogen, once separated, last for a long time, they are normally not available commercially; therefore, they must be prepared as needed. A time-proven process for the enrichment of parahydrogen follows a procedure first described by Bonhoeffer and Harteck [18]. This is based upon the fact that, at low temperature, the energetically more favorable isomer

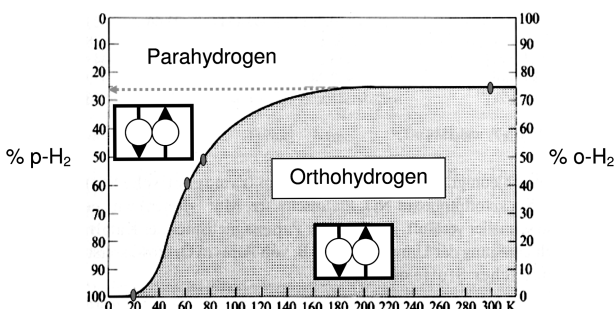


Fig. 12.5 Fraction of spin isomers at thermal equilibrium between o-H<sub>2</sub> and p-H<sub>2</sub>.

(i.e., parahydrogen) becomes enriched, provided that a suitable catalyst renders the conversion possible. In this respect, activated charcoal functions as a convenient catalyst.

### 12.2.3.2 High-Pressure Apparatus for Parahydrogen Enrichment

The apparatus used (Fig. 12.6) follows the Bonhoeffer and Harteck concept [18]. Using liquid nitrogen as a coolant, it produces a constant flow of a mixture of 51% parahydrogen and 49% orthohydrogen (i.e., 51% enriched parahydrogen), at pressures up to 20 bar. As such it is especially suited for NMR investigations at elevated pressures using recently developed NMR probes [4]. The U-shaped charcoal reactor A shown in Figure 12.7 is manufactured from brass tubing, 4 cm in diameter and 30 cm in height, and capable of withstanding pressures of 20 bar and more. Copper tubing (3 mm) is used throughout to connect the reactor with the pressure relief valve (P) and the other components of the apparatus. The reactor is filled up to two-thirds of its height with coarse-grained charcoal, which is topped off with glass wool to constrain the filling. It is not advantageous to use powdered charcoal, as this tends to restrict the flow of the hydrogen through the reactor. Furthermore, tiny particles of charcoal are then carried along by the gas and drift into other parts of the apparatus.

In order to prime the apparatus, the charcoal-filled reactor is initially heated to 400 °C and maintained at this temperature for 10 h while operating the vacuum pump. This procedure must be repeated subsequently at regular intervals in order to regenerate the charcoal filling. The so-activated charcoal removes contaminants from the hydrogen stream, and thereby also serves as a gas cleaner.

Upon appropriate priming, the activated charcoal reactor A must be evacuated and is subsequently chilled in a liquid nitrogen bath. After an induction period, which depends on the operating pressure, 51% enriched parahydrogen is avail-

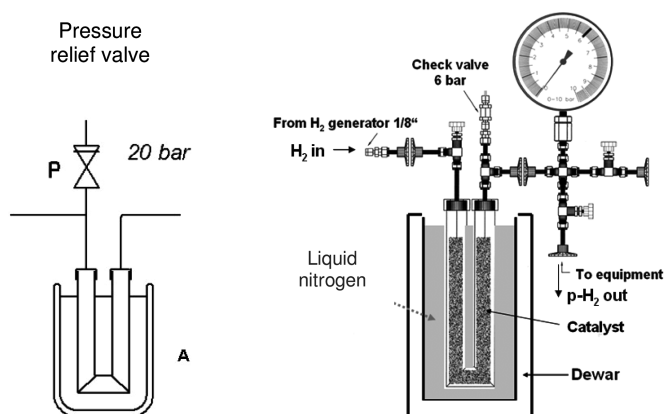


Fig. 12.6 Apparatus for the enrichment of parahydrogen at high pressure; principle and details.



able and can be supplied continuously. Typical induction periods are 30 min at 1 bar hydrogen pressure and 60 min at 10 bar. Flow rates of  $50 \text{ mL min}^{-1}$  have been achieved and tested in this mode, without any loss of parahydrogen enrichment during a prolonged flow period.

Upon termination of the experiment, all parts of the apparatus should be evacuated once again, before the liquid nitrogen bath is removed. The same precaution should also be maintained during removal of the bath, in order to safeguard against pressure surges caused by thermal expansion of the residual hydrogen or due to sudden desorption from the charcoal.

Integrated thermal conductivity cells (see Fig. 12.8) allow a quantitative determination of the corresponding ortho/para ratios of the dihydrogen. The enriched parahydrogen is well-suited for *in-situ* NMR studies of hydrogenation reactions that yield nuclear spin polarization due to symmetry breaking during the reaction. The same apparatus has also been used successfully to enrich ortho- and paradeuterium mixtures.

### 12.2.3.3 Enrichment of Parahydrogen using Closed-Circuit Cryorefrigeration

Virtually pure parahydrogen can conveniently be obtained upon cooling molecular hydrogen to temperatures between 20 and 30 K. For this purpose, commercially manufactured systems are available, and details have been described elsewhere [52]. It is advantageous (for thermodynamic considerations) and preferable (for safety reasons) to maintain the cooling temperature above the boiling point of dihydrogen at the corresponding pressure; therefore, the cryo-system should be operated at ca. 30 K. The level of enrichment for parahydrogen at 1.5 bar and flow rates of 10 to  $30 \text{ mL min}^{-1}$  for the two systems operating at 30 or 77 K, respectively, is illustrated in Figure 12.7.

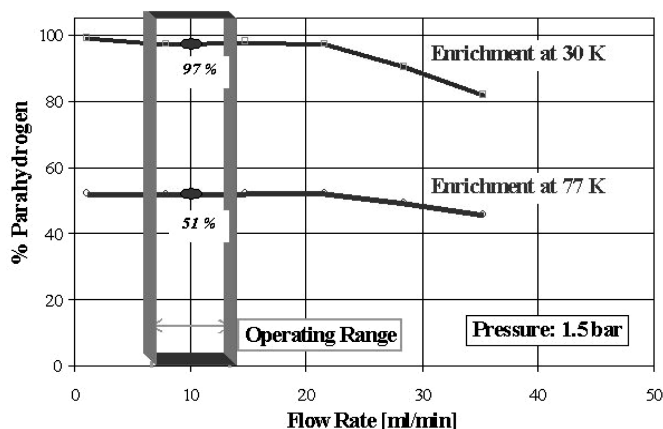


Fig. 12.7 Enrichment of parahydrogen as a function of temperature and flow rate.

## 12.2.4

**Preparation of Orthohydrogen**

During the 1950s, the enrichment or isolation of orthohydrogen was occasionally assumed to be impossible [19], until Sandler [10] described a procedure based on the preferential adsorption of the ortho form of dihydrogen on diamagnetic surfaces at low temperatures. The energy difference of orthohydrogen between its free and adsorbed state can be explained using the model of the hindered rotator [53]. Cunningham et al. [54] have presented an apparatus for the enrichment of orthohydrogen up to 99% using carefully selected  $\gamma$ -alumina in a cascade of selective desorption at 20.4 K. The present author's group have used single-stage separation of orthohydrogen on  $\gamma$ -alumina at 77 K (liquid nitrogen), and routinely obtained a mixture of 15% parahydrogen and 85% orthohydrogen (i.e., 85% enriched orthohydrogen), which is sufficient for most purposes [17]. Since the enrichment of orthohydrogen is carried out at ambient pressure, it is superfluous to design this apparatus for higher pressures. The alumina adsorption cell (B in Fig. 12.8) forms the core of the low-pressure apparatus. This cell is designed as a glass tube helix, and is fabricated from 150 cm of 20-mm diameter glass tubing. The helix provides for a rapid and homogeneous temperature change using a Dewar flask containing liquid nitrogen. This helix is charged with 260 g of  $\gamma$ -alumina that must not contain paramagnetic impurities (E. Merck, Darmstadt, Germany, Art. # 1095) [55]. The helix is terminated with fritted glass, through which it is connected to the remainder of the all-glass apparatus. Prior to the first orthohydrogen enrichment the  $\gamma$ -alumina filling is activated and degassed at 400 °C for 10 h, similar to the process described for the activated charcoal filling. Batches of orthohydrogen enriched to 85% can be prepared in this low-pressure apparatus, and the degree of enrichment can be determined accurately using thermal conductivity cells.

## 12.2.5

**Thermal Conductivity Cells for Ortho/Para Determination**

A pair of thermal conductivity cells (C in Fig. 12.8) according to Grilly [56] is used to determine the ortho/para ratio. Each cell is constructed from 120 mm of 10-mm diameter glass tubing, whereby two VACON pins lead into the interior carrying a tungsten filament, which is aligned along the center axis of the cell. Electrically, the filaments of the two cells form a bridge circuit together with appropriate resistors, which can be balanced externally. For maximum sensitivity reasons their resistance should be of the same order of magnitude as the filament resistance. The bridge voltage (here 25 V) is chosen such that the filaments heat up to 250 K, since under these conditions the resulting temperature gradient between the filaments and the walls of the liquid nitrogen-chilled cells is appropriately within the range of optimum sensitivity and performance.

The thermal conductivity cells are connected to their respective valves V1 and V2, using U-shaped glass tubing. This design has been found advantageous, as it minimizes any unavoidable convection of hydrogen within the cells.

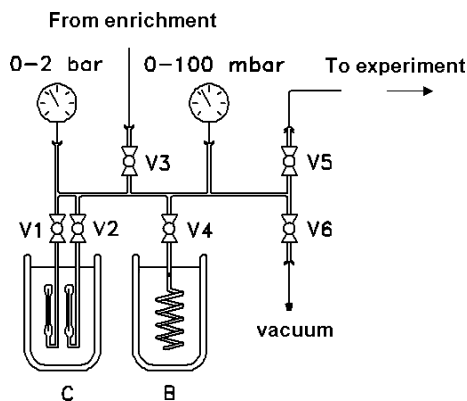


Fig. 12.8 Apparatus for orthohydrogen enrichment at low pressure, and integrated thermal conductivity cells.

### 12.2.6

#### Determination of the Ortho/Para Ratio

The specific heats of ortho- and parahydrogen differ one from another, whereby the difference reaches a maximum at temperatures in between 140 and 170 K. Within this temperature range the difference between heat capacities is sufficient and suitable to determine the ortho/para ratio of  $H_2$  using thermal conductivity cells. Typically, the setup according to Grilly is used; this consists of two conductivity cells, whereby one functions as a reference to eliminate long-term thermal drift [56]. The resistance of the tungsten filament in these cells is almost proportional to the orthohydrogen concentration [57]; therefore, it can be used as a measure for the ortho/para ratio.

### 12.2.7

#### Enrichment of Ortho- or Paradeuterium

Using the same apparatus, molecular deuterium ( $D_2$ ) can also be enriched in its ortho- or para-forms. It must be noted, however, that in the case of  $D_2$  the ortho-form is the energetically more favorable and hence easier to prepare [19]. Therefore, it is orthodeuterium which becomes enriched when using an appropriately cooled charcoal cell. The achievable degree of enrichment at the temperature of liquid nitrogen (77 K) is considerably lower than in the case of  $H_2$ , but nonetheless the apparatus has been used successfully for the enrichment of the  $D_2$  spin isomers, albeit with appropriate modifications of the procedure. Essentially, in this case the Dewar flask to be filled with liquid nitrogen should tolerate a partial vacuum (underpressure) because, by lowering the pressure of the boiling nitrogen, the temperature falls, and eventually the nitrogen solidifies somewhere at around 60 K. This temperature suffices to achieve an adequate enrichment to observe orthodeuterium-induced polarization (ODIP) [46].

Far superior results have been obtained, however, using closed-circuit cryorefrigeration for the required cooling of the  $D_2$ , as this allows the temperature to

be lowered to 20–30 K. In this case, when determining the enrichment the resistors of the bridge circuit and the operating temperature of the thermal conductivity cells must be optimized for D<sub>2</sub>, due to the different physical parameters of its individual spin isomers [52].

### 12.3

#### Applications of PHIP-NMR Spectroscopy

##### 12.3.1

##### *In-Situ* PHIP-NMR Spectroscopy of Homogeneous Hydrogenations

###### 12.3.1.1 Activation of Dihydrogen

Dihydrogen shows a weak tendency to undergo chemical reactions, unless it is activated by certain types of transition-metal compounds. Buntkowsky et al. [21] have investigated the early stages of activation of H<sub>2</sub> using parahydrogen, and the results and conclusions derived thereof have been reported.

In general, the activation of dihydrogen by transition-metal complexes has been investigated intensely since the 1960s, when Wilkinson and colleagues discovered the first successful homogeneous hydrogenation catalyst RhCl(PPh<sub>3</sub>)<sub>3</sub> [22]. Herewith, terminal alkenes and alkynes can be readily hydrogenated at 25 °C at a hydrogen pressure of 1 bar. The mechanism and kinetics thereof have since been extensively studied. Some intermediate dihydrides such as Rh(H)<sub>2</sub>Cl(PPh<sub>3</sub>)<sub>3</sub> and Rh(H)<sub>2</sub>Cl<sub>2</sub>(PPh<sub>3</sub>)<sub>4</sub> have been previously observed and characterized using NMR spectroscopy [23], and even PHIP-NMR spectroscopy [24].

The data available in the literature, however, are typically restricted to those containing PPh<sub>3</sub> as the phosphine ligands. In general, the spectroscopic observation of such dihydride species is rather difficult. Due to their intermediate character they have a short lifetime, and hence they typically occur only at rather low concentrations. Whereas conventional NMR spectroscopy frequently fails to identify their existence, PHIP has allowed the detection of several new dihydride products, even at these low concentrations. If hydrogenation with parahydrogen is carried out *in situ* using a spectrometer-activated apparatus, the kinetic constants of the reactions of the formation and disappearance of intermediates may be determined; details of this method are outlined in the following section.

###### 12.3.1.2 Concepts of Reaction Mechanisms

Time-proven concepts for the reaction mechanisms of homogeneous hydrogenations follow two approaches which, according to Halpern's step-wise analysis of hydrogenations using "Wilkinson's catalyst" [25] and the cationic catalyst DI-PHOS [26], respectively, can be grouped into the so-called "dihydride" or "unsaturated" routes [27] (Fig. 12.9).

Due to these alternatives, the detection of intermediates is of considerable interest, as this would allow differentiation to be made between these two principal al-

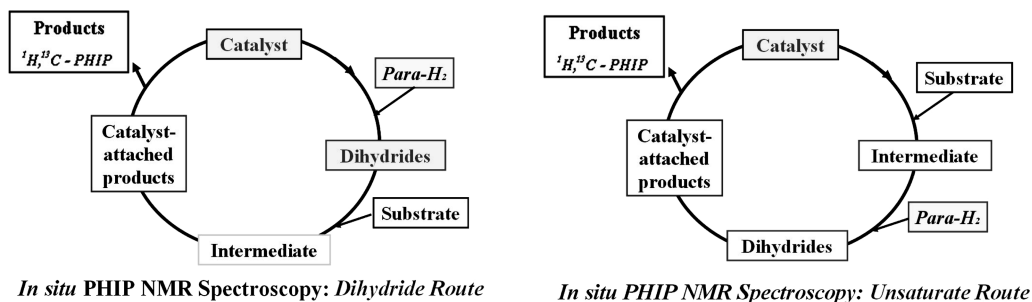


Fig. 12.9 Alternative approaches to the sequence of events during the catalytic activation of dihydrogen.

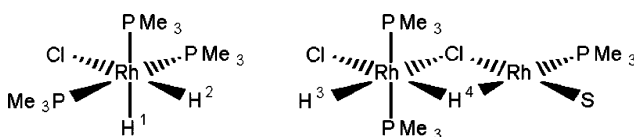


Fig. 12.10 Mono- and binuclear rhodium dihydride complexes.

ternatives. Evidence in favor of one or the other route has been accumulated and associated with the nature of the catalysts – that is, whether they are cationic or neutral – and extensive accounts of this have been published. Within the scope of this chapter, a number of special cases will be discussed that provide evidence for the existence of different intermediates, including a number of dihydrides.

### 12.3.2

#### *In-Situ* PHIP-NMR Observation of Mono- and Binuclear Rhodium Dihydride Complexes

PHIP can also be used to identify and characterize mono- and binuclear rhodium dihydride complexes such as  $[\text{RhH}_2\text{ClL}_3]$  ( $\text{L} = \text{PMe}_3, \text{PMe}_2\text{Ph}, \text{PMePh}_2, \text{PEt}_3, \text{PEt}_2\text{Ph}, \text{PEtPh}_2,$  or  $\text{P}(n\text{-butyl})_3$ ),  $[(\text{H})(\text{Cl})\text{Rh}(\text{PMe}_3)_2(\mu\text{-Cl})(\mu\text{-H})\text{Rh}(\text{PMe}_3)]$ , and  $[(\text{H})(\text{Cl})\text{Rh}(\text{PMe}_2\text{Ph})_2(\mu\text{-Cl})(\mu\text{-H})\text{Rh}(\text{PMe}_2\text{Ph})]$  (Fig. 12.10) obtained from the binuclear complex  $[\text{RhCl}(2,5\text{-norbornadiene})]_2$  when treated with the corresponding phosphine and parahydrogen. By substituting chloride with trifluoroacetate, the complexes  $[\text{RhH}_2(\text{CF}_3\text{COO})\text{L}_3]$  ( $\text{L} = \text{PPh}_3, \text{PEt}_2\text{Ph}, \text{PEt}_3,$  and  $\text{P}(n\text{-butyl})_3$ ) are analogously generated [58].

#### 12.3.2.1 Reactions of $[\text{RhCl}(\text{NBD})]_2$ with Parahydrogen in the Presence of Tertiary Phosphines

The binuclear precursor (di- $\mu$ -chloro-bis- $[\eta^4\text{-}2,5\text{-norbornadiene}]$ -rhodium(I)) =  $[(\text{Rh}(\text{NBD})\text{Cl})_2]$  is well suited for the *in-situ* preparation of a variety of homogeneous hydrogenation catalysts, if tertiary phosphines (here:  $\text{PMe}_3, \text{PMe}_2\text{Ph}$ ,

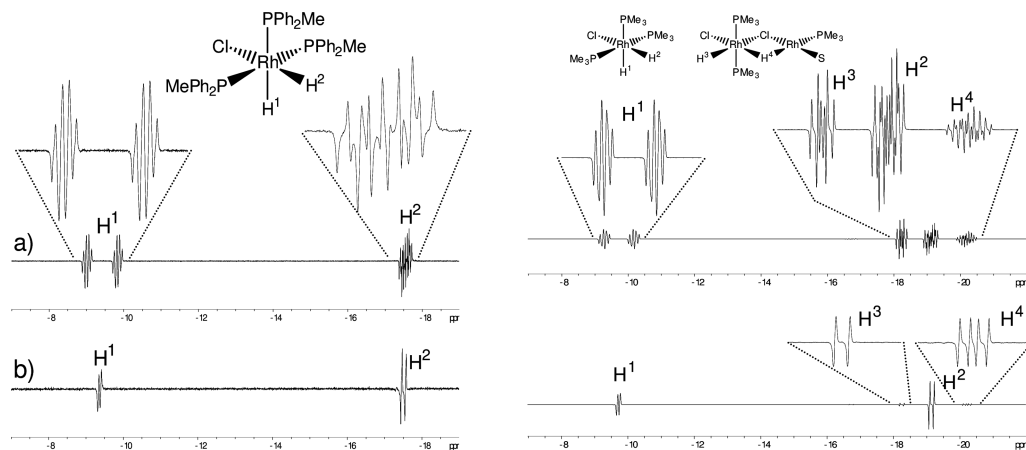


Fig. 12.11 PHIP-NMR spectra of some mono- (left) and binuclear Rh-complexes (right).

PMePh<sub>2</sub>, PEt<sub>3</sub>, PEt<sub>2</sub>Ph, PEtPh<sub>2</sub>, or P(*n*-butyl)<sub>3</sub> are added. Upon the addition of dihydrogen to solutions of these mixtures, NBD is hydrogenated off, and mono-nuclear dihydride species [Rh(H)<sub>2</sub>ClL<sub>3</sub>] are generated, most likely via the complexes [RhClL<sub>3</sub>] as intermediates. These dihydride complexes play a key role as intermediates in any subsequent catalytic hydrogenation.

As characteristic examples, Figure 12.11 (left) shows the results obtained upon addition of parahydrogen to a solution of 10 mg [Rh(NBD)Cl]<sub>2</sub> and 19  $\mu$ L PMePh<sub>2</sub> in acetone-d<sub>6</sub> (Rh:P=1:3). Strongly enhanced resonances of the dihydride protons of the complex [Rh(H)<sub>2</sub>Cl(PMePh<sub>2</sub>)<sub>3</sub>] are observed in the <sup>1</sup>H-NMR spectrum, whereby the hydride *trans* to a PMePh<sub>2</sub> ligand occurs at  $\delta_{\text{H}} = -9.4$  ppm, whereas the hydride *trans* to the chloride has a higher chemical shift and appears at  $\delta_{\text{H}} = 17.6$  ppm. The latter is characteristic for hydride protons in the *trans* position to such an electronegative ligand. The hydride resonance at lower field shows a large coupling to one *trans* phosphorus ( $J_{\text{HP}(\text{trans})} = 178.6$  Hz), an additional coupling to two equivalent *cis* phosphorus nuclei ( $J_{\text{HP}(\text{cis})} = 14.1$  Hz), a coupling to the central rhodium ( $J_{\text{HRh}} = 13$  Hz), and a coupling to the upfield hydride proton ( $J_{\text{HH}'} = -7.7$  Hz).

The coupling between the two former parahydrogen protons causes the anti-phase character of this resonance, exhibiting emission and absorption maxima, accordingly. The second hydride resonance at higher field is a complex multiplet with couplings to rhodium ( $J_{\text{HRh}} = 22$  Hz), one equatorial and two axial phosphorus nuclei ( $J_{\text{HP}(\text{ax.})} = 16.5$  Hz,  $J_{\text{HP}(\text{eq.})} = 11$  Hz), and the lower field hydride proton ( $J_{\text{HH}'} = -7.7$  Hz). These data have been tested by simulating the resulting multiplet and its polarization pattern using the computer program PHIP<sup>++</sup>, upon which very good agreement has been obtained [28].

If the <sup>1</sup>H-NMR spectrum is recorded with complete <sup>31</sup>P decoupling, both hydride resonance at  $-9.4$  ppm and  $-17.6$  ppm collapse into a doublet of antiphase doublets. The remaining 13-Hz and 22-Hz couplings correspond to  $J_{\text{HRh}}$  and  $J_{\text{HRh}}$ ,

Table 12.1  $^1\text{H}$ -NMR data of the observed hydrides.

No.	Complex	$^1\text{H}$ chemical shifts $\delta$ [ppm] in acetone- $d_6$ and coupling constants J [Hz]
1	$[\text{Rh}(\text{H})_2\text{Cl}(\text{PMe}_3)_3]$	$-9.7$ ( $^1J_{\text{HRh}} = 15$ , $^2J_{\text{HP}(\text{trans})} = 178.6$ , $^2J_{\text{HP}(\text{cis})} = 20$ , $^2J_{\text{HH}} = -7.5$ ) $-19.0$ ( $^1J_{\text{HRh}} = 27$ , $^2J_{\text{HP}(\text{ax})} = 19$ , $^2J_{\text{HP}(\text{eq})} = 13$ , $^2J_{\text{HH}} = -7.5$ )
2	$[\text{Rh}(\text{H})_2\text{Cl}(\text{PMe}_2\text{Ph})_3]$	$-9.6$ ( $^1J_{\text{HRh}} = 18$ , $^2J_{\text{HP}(\text{trans})} = 172.5$ , $^2J_{\text{HP}(\text{cis})} = 18$ , $^2J_{\text{HH}} = -7.2$ ) $-18.2$ ( $^1J_{\text{HRh}} = 24.7$ , $^2J_{\text{HP}(\text{ax})} = 16.5$ , $^2J_{\text{HP}(\text{eq})} = 11$ , $^2J_{\text{HH}} = -7.2$ )
3	$[\text{Rh}(\text{H})_2\text{Cl}(\text{PMePh}_2)_3]$	$-9.4$ ( $^1J_{\text{HRh}} = 13$ , $^2J_{\text{HP}(\text{trans})} = 164$ , $^2J_{\text{HP}(\text{cis})} = 14.1$ , $^2J_{\text{HH}} = -7.7$ ) $-17.6$ ( $^1J_{\text{HRh}} = 22$ , $^2J_{\text{HP}(\text{ax})} = 15$ , $^2J_{\text{HP}(\text{eq})} = 10$ , $^2J_{\text{HH}} = -7.7$ )
4	$[\text{Rh}(\text{H})_2\text{Cl}(\text{PEt}_3)_3]$	$-10.7$ ( $^1J_{\text{HRh}} = 14.7$ , $^2J_{\text{HP}(\text{trans})} = 161.7$ , $^2J_{\text{HP}(\text{cis})} = 16$ , $^2J_{\text{HH}} = -7.9$ ) $-19.8$ ( $^1J_{\text{HRh}} = 24.1$ , $^2J_{\text{HP}(\text{ax})} = 16$ , $^2J_{\text{HP}(\text{eq})} = 13$ , $^2J_{\text{HH}} = -7.9$ )
5	$[\text{Rh}(\text{H})_2\text{Cl}(\text{PEt}_2\text{Ph})_3]$	$-10.1$ ( $^1J_{\text{HRh}} = 15.4$ , $^2J_{\text{HP}(\text{trans})} = 162$ , $^2J_{\text{HP}(\text{cis})} = 16.3$ , $^2J_{\text{HH}} = -7.3$ ) $-19.3$ ( $^1J_{\text{HRh}} = 24.6$ , $^2J_{\text{HP}(\text{ax})} = 17$ , $^2J_{\text{HP}(\text{eq})} = 15.1$ , $^2J_{\text{HH}} = -7.3$ )
6	$[\text{Rh}(\text{H})_2\text{Cl}(\text{PEtPh}_2)_3]$	$-9.9$ ( $^1J_{\text{HRh}} = 12.5$ , $^2J_{\text{HP}(\text{trans})} = 155$ , $^2J_{\text{HP}(\text{cis})} = 13.3$ , $^2J_{\text{HH}} = -7.9$ ) $-18.3$ ( $^1J_{\text{HRh}} = 20$ , $^2J_{\text{HP}(\text{ax})} = 12.5$ , $^2J_{\text{HP}(\text{eq})} = 13.5$ , $^2J_{\text{HH}} = -7.9$ )
7	$[\text{Rh}(\text{H})_2\text{Cl}(\text{P}(n\text{-butyl})_3)_3]$	$-10.7$ ( $^1J_{\text{HRh}} = 13.5$ , $^2J_{\text{HP}(\text{trans})} = 163$ , $^2J_{\text{HP}(\text{cis})} = 16.7$ , $^2J_{\text{HH}} = -7.8$ ) $-19.8$ ( $^1J_{\text{HRh}} = 23$ , $^2J_{\text{HP}(\text{ax})} = 15.8$ , $^2J_{\text{HP}(\text{eq})} = 13.1$ , $^2J_{\text{HH}} = -7.8$ )
8	$[(\text{H})(\text{Cl})\text{Rh}(\text{PMe}_3)_2(\mu\text{-Cl})(\mu\text{-H})\text{-Rh}(\text{PMe}_3)]$	$-18.2$ ( $^1J_{\text{HRh}} = 25$ , $^2J_{\text{HP}(\text{cis})} = 17.3$ , $^2J_{\text{HH}} = -4.2$ ) $-20.2$ ( $^1J_{\text{HRh}} = 30.3$ , $^2J_{\text{HP}(\text{trans})} = 29$ , $^2J_{\text{HP}(\text{cis})} = 14.6$ , $^2J_{\text{HH}} = -4.2$ )
9	$[(\text{H})(\text{Cl})\text{Rh}(\text{PMe}_2\text{Ph})_2(\mu\text{-Cl})\text{-}(\mu\text{-H})\text{Rh}(\text{PMe}_2\text{Ph})]$	$-17.3$ ( $^1J_{\text{HRh}} = 23$ , $^2J_{\text{HP}(\text{cis})} = 15.4$ , $^2J_{\text{HH}} = -4.2$ ) $-20.0$ ( $^1J_{\text{HRh}} = 30$ , $^2J_{\text{HP}(\text{trans})} = 29$ , $^2J_{\text{HP}(\text{cis})} = 15.5$ , $^2J_{\text{HH}} = -4.2$ )
10	$[\text{Rh}(\text{H})_2(\text{CF}_3\text{COO})(\text{PPh}_3)_3]$	$-8.9$ ( $^1J_{\text{HRh}} = 6$ , $^2J_{\text{HP}(\text{trans})} = 161$ , $^2J_{\text{HP}(\text{cis})} = 12$ , $^2J_{\text{HH}} = -9.5$ ) $-19.1$ ( $^1J_{\text{HRh}} = 18$ , $^2J_{\text{HP}(\text{ax})} = 17$ , $^2J_{\text{HP}(\text{eq})} = 17$ , $^2J_{\text{HH}} = -9.5$ )
11	$[\text{Rh}(\text{H})_2(\text{CF}_3\text{COO})(\text{PEt}_3)_3]$	$-10.1$ ( $^1J_{\text{HRh}} = 14.8$ , $^2J_{\text{HP}(\text{trans})} = 160$ , $^2J_{\text{HP}(\text{cis})} = 16$ , $^2J_{\text{HH}} = -8.7$ ) $-22.5$ ( $^1J_{\text{HRh}} = 13$ , $^2J_{\text{HP}(\text{ax})} = 17$ , $^2J_{\text{HP}(\text{eq})} = 17$ , $^2J_{\text{HH}} = -8.7$ )
12	$[\text{Rh}(\text{H})_2(\text{CF}_3\text{COO})(\text{PEt}_2\text{Ph})_3]$	$-9.5$ ( $^1J_{\text{HRh}} = 15.5$ , $^2J_{\text{HP}(\text{trans})} = 161$ , $^2J_{\text{HP}(\text{cis})} = 16.8$ , $^2J_{\text{HH}} = -8.6$ ) $-21.9$ ( $^1J_{\text{HRh}} = 26.8$ , $^2J_{\text{HP}(\text{ax})} = 16.7$ , $^2J_{\text{HP}(\text{eq})} = 16.7$ , $^2J_{\text{HH}} = -8.6$ )
13	$[\text{Rh}(\text{H})_2(\text{CF}_3\text{COO})(\text{P}(n\text{-butyl})_3)_3]$	$-9.5$ ( $^1J_{\text{HRh}} = 15.5$ , $^2J_{\text{HP}(\text{trans})} = 161.5$ , $^2J_{\text{HP}(\text{cis})} = 16.7$ , $^2J_{\text{HH}} = -7.1$ ) $-21.9$ ( $^1J_{\text{HRh}} = 28.8$ , $^2J_{\text{HP}(\text{ax})} = 17.5$ , $^2J_{\text{HP}(\text{eq})} = 17.5$ , $^2J_{\text{HH}} = -7.1$ )

respectively (Fig. 12.11). Analogous complexes with other phosphine ligands have also been observed (Table 12.1). If the temperature is elevated, the intensities of the polarized hydride resonances increase significantly. The spectrum displayed in Figure 12.11 was recorded at 315 K. Experiments in acetone- $d_6$  can be carried out up to about 330 K, since above this value, boiling and associated evaporation of the solvent becomes so significant that this badly interferes with the quality of the spectra. Furthermore, the resolution of the corresponding hydride resonances deteriorates with increasing temperature. Therefore, a lower temperature is advantageous for better resolution, since the rate of phosphine dissociation slows down with decreasing temperature, upon which the resonances sharpen.

The rate of the observed exchange reaction of the phosphine ligands in the dihydrides increases in the above-listed series of phosphines from  $\text{PMe}_3$  to  $\text{P}(n\text{-butyl})_3$  (Table 12.1), which in turn correlates with the activity of the corresponding complexes as hydrogenation catalysts.

Furthermore, the intensities of the polarized hydride resonances increase with temperature. Since these intensities correlate with the rate of the oxidative addi-

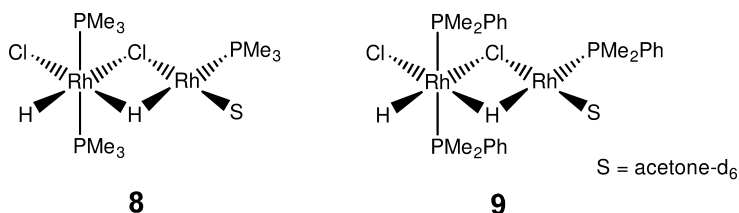
tion of parahydrogen to the corresponding Rh complexes and with the subsequent decay of the so-formed dihydrides, both the rates of their formation as well as the rates of their decay seem to increase with temperature.

### 12.3.2.2 Formation of the Binuclear Complexes [(H)(Cl)Rh(PMe<sub>3</sub>)<sub>2</sub>(μ-Cl)- (μ-H)Rh(PMe<sub>3</sub>)] and [(H)(Cl)Rh(PMe<sub>2</sub>Ph)<sub>2</sub>(μ-Cl)(μ-H)Rh(PMe<sub>2</sub>Ph)]

Upon the addition of parahydrogen to a solution of [RhCl(NBD)]<sub>2</sub> and PMe<sub>3</sub> (ratio of Rh:P=1:3) in acetone-d<sub>6</sub> at 315 K, intense polarization signals of the dihydride complex [Rh(H)<sub>2</sub>Cl(PMe<sub>3</sub>)<sub>3</sub>] (**1**) can be observed, together with strongly polarized resonances in the aliphatic region due to hydrogenation of the NBD ligand. This complex **1** has also been investigated by others using PHIP-NMR spectroscopy [29]. In the later stages of the reaction, however, two new resonances emerge at -18.2 ppm and -20.2 ppm, respectively (Fig. 12.11, right), which can be assigned to the hydride protons of the complex **8** (Scheme 12.1). These signals also have antiphase character due to coupling between the two parahydrogen protons ( $J_{\text{HH}'} = -4.2$  Hz). Thereby, the hydride resonance at -18.2 ppm exhibits a coupling to Rh ( $J_{\text{HRh}} = 25$  Hz) and the *cis* phosphorus ( $J_{\text{HP}(\text{cis})} = 17.3$  Hz). The second hydride resonance consists of a complex multiplet with couplings to the two inequivalent Rh atoms ( $J_{\text{HRh}} = 30.3$  Hz and  $J_{\text{Rh}'\text{H}} = 20$  Hz, respectively), as well as to the *trans* ( $J_{\text{HP}(\text{trans})} = 29$  Hz) and the two *cis* phosphorus nuclei ( $J_{\text{HP}(\text{cis})} = 14.6$  Hz). This assignment is confirmed upon <sup>31</sup>P decoupling of the hydride protons: In the <sup>1</sup>H{<sup>31</sup>P} NMR spectrum (see Fig. 12.11) the signal at -18.2 ppm has collapsed into a doublet of antiphase doublets with the 25-Hz coupling corresponding to  $J_{\text{HRh}}$ . The second hydride resonance has simplified to a doublet of doublet of antiphase doublets, with couplings of 30.3 Hz and 20 Hz corresponding to  $J_{\text{HRh}}$  and  $J_{\text{HRh}'}$ , respectively.

Complexes of the type [(H)(Cl)Rh(PMe<sub>3</sub>)<sub>2</sub>(μ-Cl)(μ-H)Rh(CO)(PMe<sub>3</sub>)] and [(H)(Cl)Rh(PMe<sub>3</sub>)<sub>2</sub>(μ-I)(μ-H)Rh(CO)(PMe<sub>3</sub>)], with NMR data corresponding to our results, have also been observed before by Duckett, Eisenberg, and co-workers, using PHIP-NMR spectroscopy [30, 31].

In these earlier studies the phosphine ligand at the rhodium(I) center has been shown to be *trans* to the μ-hydride with a phosphorus coupling of  $J_{\text{HP}(\text{trans})} = 30$  Hz and 32 Hz, respectively. Therefore, we assign to complex **8** the structure as outlined in Scheme 12.1.



Scheme 12.1



In their study of Wilkinson's catalyst, Duckett and Eisenberg postulated binuclear complexes containing an alkene at the rhodium(I) center [24].

Additional dihydride complexes can be obtained using  $\text{PEt}_3$ ,  $\text{PEt}_2\text{Ph}$ , or  $\text{P}(n\text{-butyl})_3$  as the phosphine ligands. However, in the case of  $\text{PEt}_2\text{Ph}$  or  $\text{P}(n\text{-butyl})_3$ , the resonances of the dihydrides are broadened due to a rapid exchange of these phosphine ligands, which blurs the resonances of the hydride protons. Upon cooling the sample, the rate of this exchange process can be slowed down resulting in improved resolution.

Upon using either acetic acid or tetrafluoroboric acid instead of trifluoroacetic acid, however, no analogous rhodium-containing dihydrides could be observed. A few similar Rh-containing complexes have been described before by other authors [32].

### 12.3.2.3 General Procedure for the Generation of the Complexes $[\text{Rh}(\text{H})_2\text{ClL}_3]$ (L=Phosphine)

In a typical experiment, the rhodium complex  $[\text{RhCl}(\text{NBD})]_2$  (10 mg) and the corresponding amount of phosphine ligand (Rh:P=1:3) are placed into an NMR tube together with 700  $\mu\text{L}$  of degassed acetone- $\text{d}_6$  (Scheme 12.2).  $p\text{-H}_2$  is then bubbled *in situ* through the solution within the magnetic field of the spectrometer, using a thin capillary that can be lowered into the spinning NMR tube. This lowering is synchronized by the NMR spectrometer, whereby the spectra are recorded not until the capillary is raised again and the  $p\text{-H}_2$  bubbles have vanished.

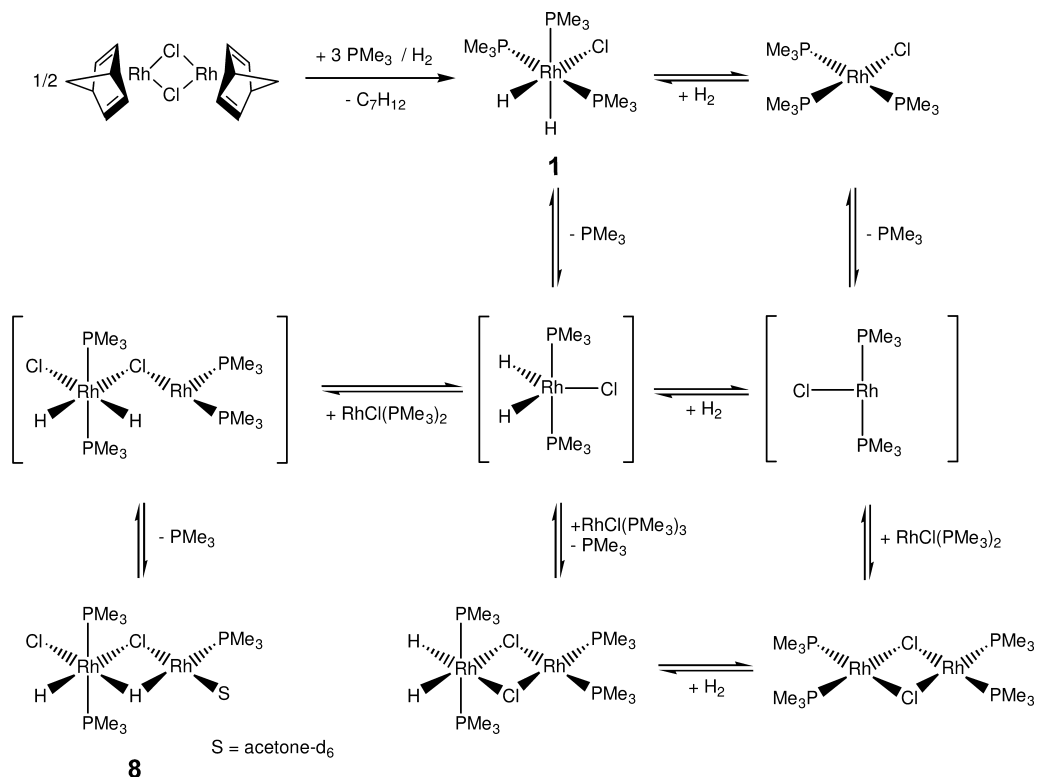
Likewise, the complex  $[\text{Rh}(\text{NBD})(\text{acac})]$  (10 mg), together with trifluoroacetic acid (1  $\mu\text{L}$ ) and a corresponding amount of phosphine ligand (Rh:P=1:3) is dissolved in 700  $\mu\text{L}$  acetone- $\text{d}_6$  and treated as described above to obtain the complexes  $[\text{Rh}(\text{H})_2(\text{CF}_3\text{COO})\text{L}_3]$  (L=phosphine).

### 12.3.3.3 Intermediate Dihydrides of Cationic Rh Catalysts

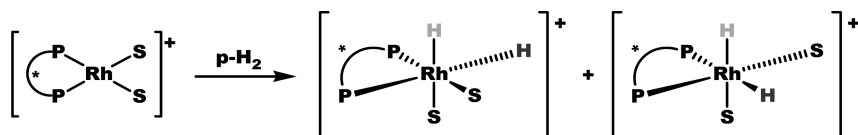
NMR evidence for intermediate dihydrides of cationic Rh catalysts remained elusive for a long time, ever since the first demonstrations [33] of effective enantioselective catalysis, for example in the homogeneous hydrogenation of dehydroamino acid derivatives for the synthesis of L-DOPA.

Para-enriched hydrogen offers considerable advantages for the NMR identification of transient intermediates [12 d, 34]. PHIP experiments carried out *in situ* under PASADENA conditions are especially powerful in this regard. The PHA-NEPHOS [MM]-derived Rh catalyst is unusually reactive, with turnover possible even at  $-40^\circ\text{C}$ . This high reactivity, coupled with good enantioselectivity, provides an ideal case for characterizing the elusive Rh dihydrides.

Upon displacement of the NBD ligand with parahydrogen according to Scheme 12.3, the  $^1\text{H}$ -PHIP-NMR spectra displayed in Figure 12.12 were observed, whereby the details of their parameters depended on the type and polarity of the solvent.



**Scheme 12.2** The sequence of reactions leading to the observed intermediates.



**Scheme 12.3** Formation of dihydride intermediates of a cationic Rh complex via displacement of the NMD ligand in the DIPHOS-derived catalyst (S=solvent).

Upon addition of dehydroamino acid esters, the Rh complexes from the above-illustrated NBD-precursor formed *in situ* with displacement of the solvents even at  $-40^{\circ}\text{C}$ . Using differently substituted substrates and mixtures thereof, the spectra shown in Figure 12.13 were observed.

The relative shift of the resonances of the dihydride nuclei listed in Table 12.2 follow a free energy correlation, as is outlined in the Hammett plots shown in Figure 12.14.

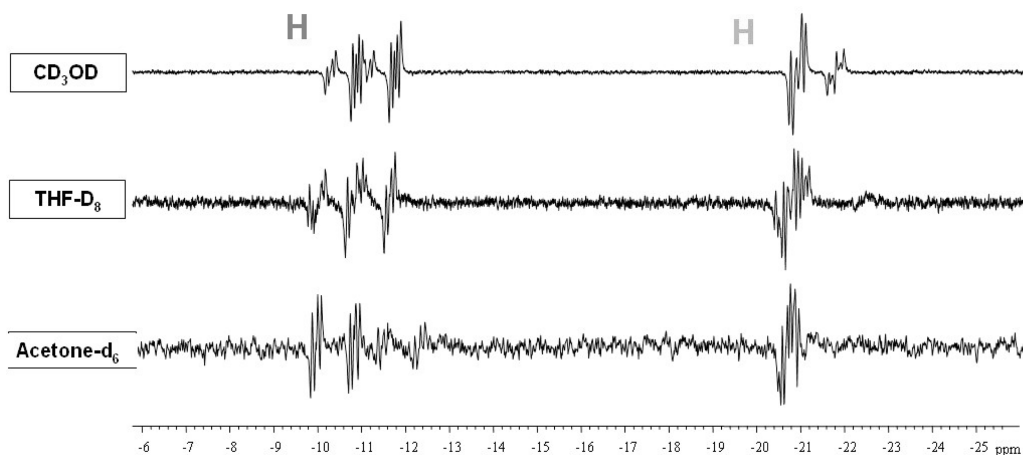


Fig. 12.12 Cationic Rh-dihydrides derived from  $[\text{Rh}(\text{NBD})(\text{DIPHOS})]^+$ .

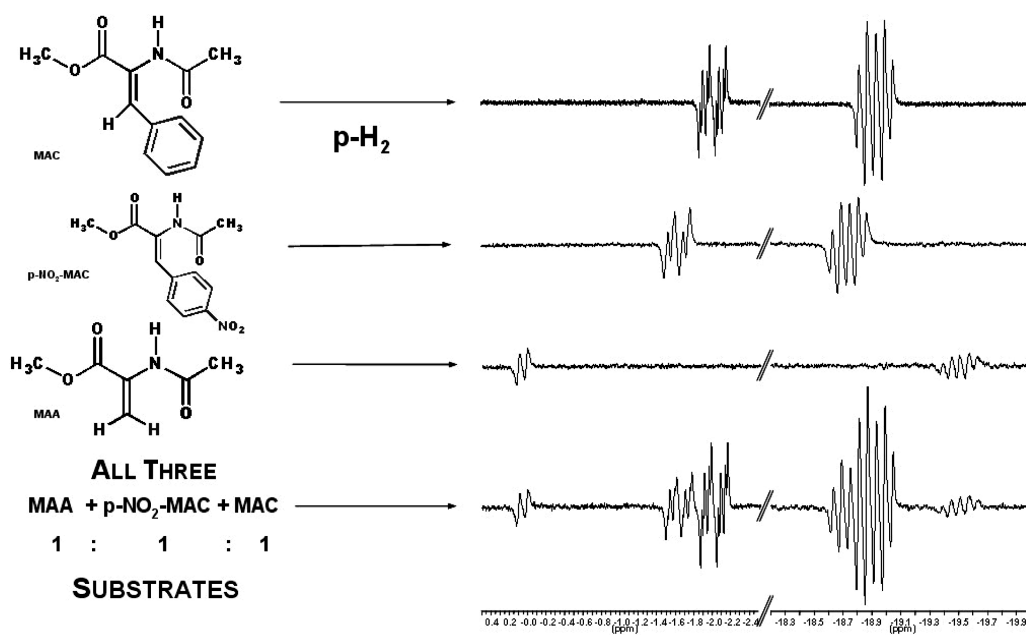
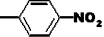




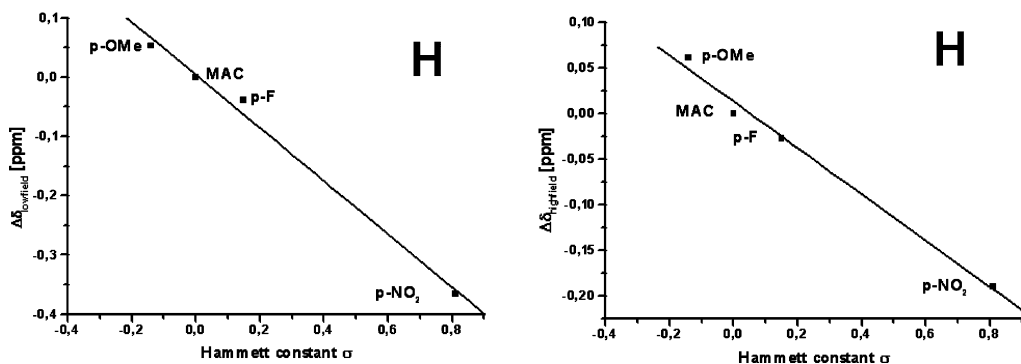
Fig. 12.13 Simultaneous  $^1\text{H}$ -PHIP-NMR spectra of dihydrides from enamide complexes of the DIPHOS-containing Rh-catalyst.

**Table 12.2** NMR data and substituent effects of the observed dihydride intermediates.

R	H			
$\delta_{\text{H}}$	+0.07 ppm	-1.60 ppm	-1.93 ppm	-1.97 ppm
$^2J_{\text{HH}}$	-1.0 Hz	-3.0 Hz	-4.3 Hz	-4.3 Hz
$^1J_{\text{HRh}}$	1.0 Hz	14.2 Hz	15 Hz	13.4 Hz
$^2J_{\text{HP}}$	17.5 Hz	32.8 Hz	36.0 Hz	34.0 Hz
	1.0 Hz	5.25 Hz	6.5 Hz	5.8 Hz

 $^1J_{\text{H}^{13}\text{C}} = 85.8 \text{ Hz}$ 

Substituent	$\sigma^{\circ}$	$\Delta\delta_{\text{LF}}$ [ppm]	$\Delta\delta_{\text{HF}}$ [ppm]
p-OMe	-0.14	+0.052	+0.061
p-F	+0.15	-0.038	-0.028
p-NO <sub>2</sub>	+0.81	-0.366	-0.190

**Fig. 12.14** Free energy correlation and Hammett plot of chemical shift data of the intermediate dihydrides.

#### 12.3.3.4 Obtaining Structural Information using $^{13}\text{C}$ -Labeled Substrates

By conducting experiments with the  $\beta$ - $^{13}\text{C}$ -labeled ester outlined in Figure 12.15, an additional  $^{13}\text{C}$  coupling of 86 Hz to the low-field Rh hydride can be detected. In addition to the expected polarization transfer to the  $^{13}\text{CH}_2\text{Ph}$  of the product at 38 ppm, a strong reactant signal appears in the  $^{13}\text{C}$  INEPT(+ $\pi/4$ ) spectrum at 135 ppm, implying reversibility of enamide complexation in the observed transient. With the  $\alpha$ - $^{13}\text{C}$ -labeled enamide, however, weak  $^{13}\text{C}$  coupling (ca. 3 Hz) to the low-field hydride is observed [35].

The experimental result and the simulated spectrum are shown in Figure 12.16. The spectroscopic data of this intermediate allows the structure and geo-

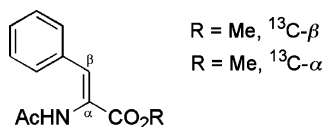


Fig. 12.15  $\beta$ - $^{13}\text{C}$ -labeled esters used as substrates.

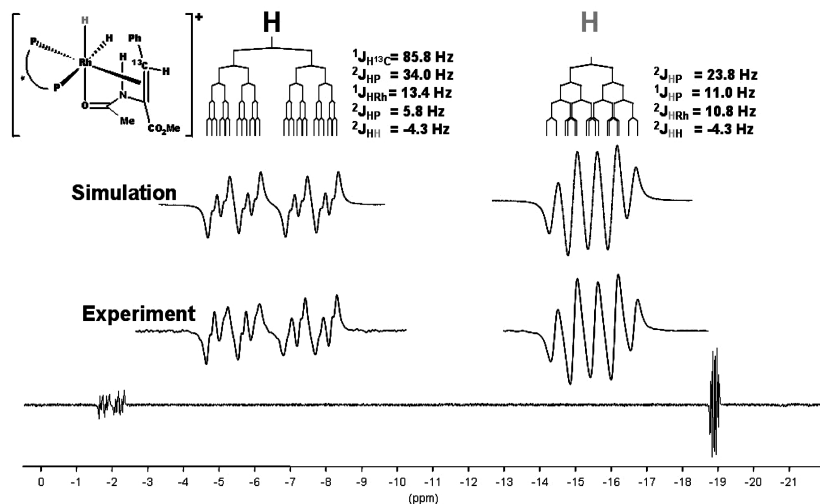


Fig. 12.16  $^1\text{H}$ -NMR spectrum of the dihydride of the enamide Rh complex.

metric details of this intermediate to be predicted. These postulates agree well with the results of high-level density functional theory (DFT) calculations. According to such calculations on the simple  $[\text{Rh}(\text{PH}_3)_2]$  complex [36], the reaction proceeds through a  $\eta^2$ -dihydrogen complex to a classical dihydride. The thermodynamically favored Rh diastereomer of this dihydride has a low energy pathway to an agostic species closely resembling the agostic dihydride intermediate outlined in Figure 12.17, although this is not on the computationally preferred pathway of hydrogenation. More specific DFT calculations [36] on the model dehydroamino ester indicate that the structure outlined in Figure 12.17 represents a significant minimum, with a computed Rh–H bond length of 1.76 Å [35, 36].

Whereas, from all of these informative  $^1\text{H}$ -PHIP-NMR spectra, the structure of the dihydride intermediate (including geometric details about peculiar bonding therein) can be determined rather exactly and reliably, a degree of uncertainty remains as to whether this intermediate represents the “major” or the “minor” diastereomer according to the nomenclature of Halpern [27]. This is the consequence of different kinetic constants associated with the two alternative cycles with different stereochemistry, and which accounts for the “major” and “minor” reaction product (Fig. 12.18). In fact, it is the difference in the rate

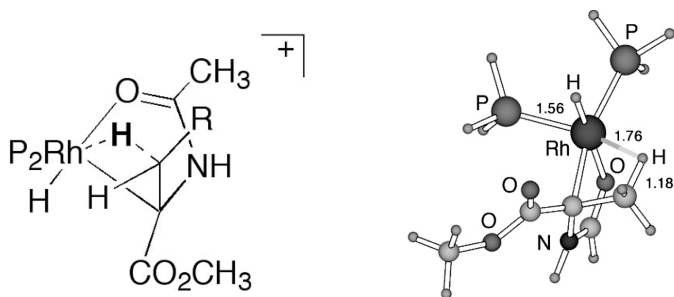


Fig. 12.17 Agostic dihydride intermediate derived from a dehydroamino ester substrate.

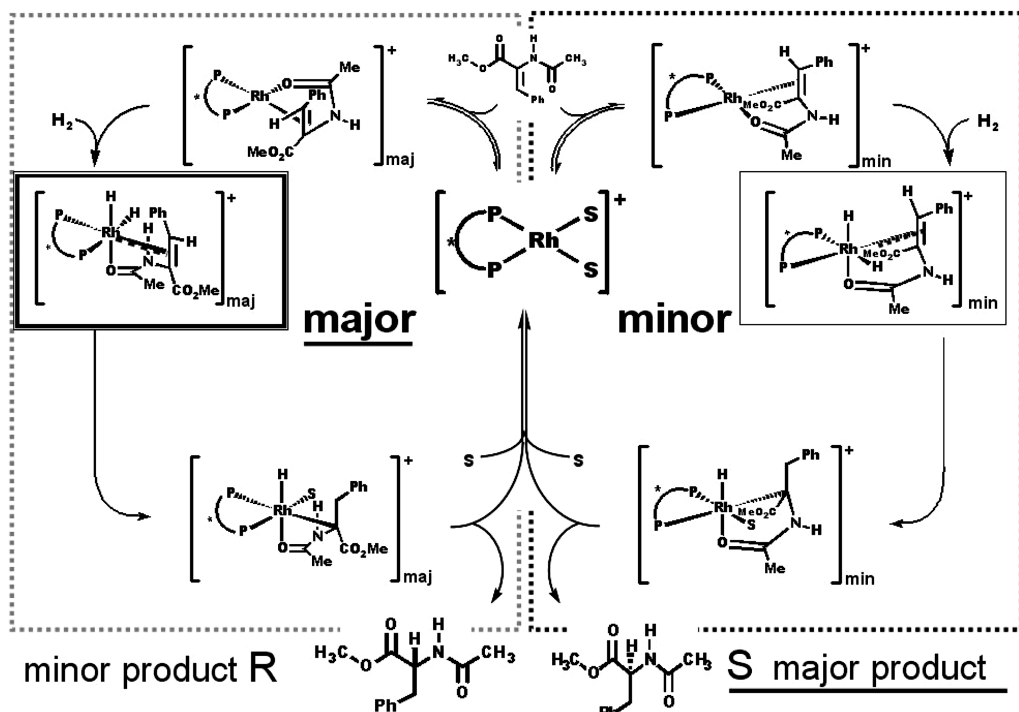


Fig. 12.18 The two equivalent but stereochemically different reaction cycles of homogeneous hydrogenation correlating the “minor” intermediate with the “major” reaction product, and vice-versa (according to [27]).

of generation and the rate of decay of the two respective intermediates that accounts for their respective lifetimes and concentrations.

In consequence, the “major” intermediate (which, in principle, is easier to detect because it should occur at a somewhat higher concentration) correlates with the “minor” reaction product, which is the irrelevant one for most synthetic purposes. The opposite is true for the “minor” intermediates, which correlate with

the “major” reaction product. Although of course the latter two are of more importance, it remains unclear as to which intermediate is seen here – the “minor”, more difficult to detect, or (more likely) the “major” intermediate [35].

#### 12.4 Catalyst-Attached Products as Observable Intermediates

During the homogeneous hydrogenation of a variety of substrates – and in particular of those containing aryl groups – “satellites” appear in addition to the “expected” PHIP-NMR spectra of the usual para-hydrogenated products, typically shifted upfield relative to those of the authentic parent compounds [37].

The shift correlates in magnitude with the separation of each particular group distance-wise from the aromatic moiety of the substrate or product; this points to the formation of an intermediate  $\pi$ -complex, for which the rate of formation and the rate of decay can be determined. The  $^1\text{H}$ -PHIP-NMR spectrum, as well as the anticipated intermediate product-catalyst- $\pi$ -complex observed during the hydrogenation of styrene, is outlined in Figure 12.19.

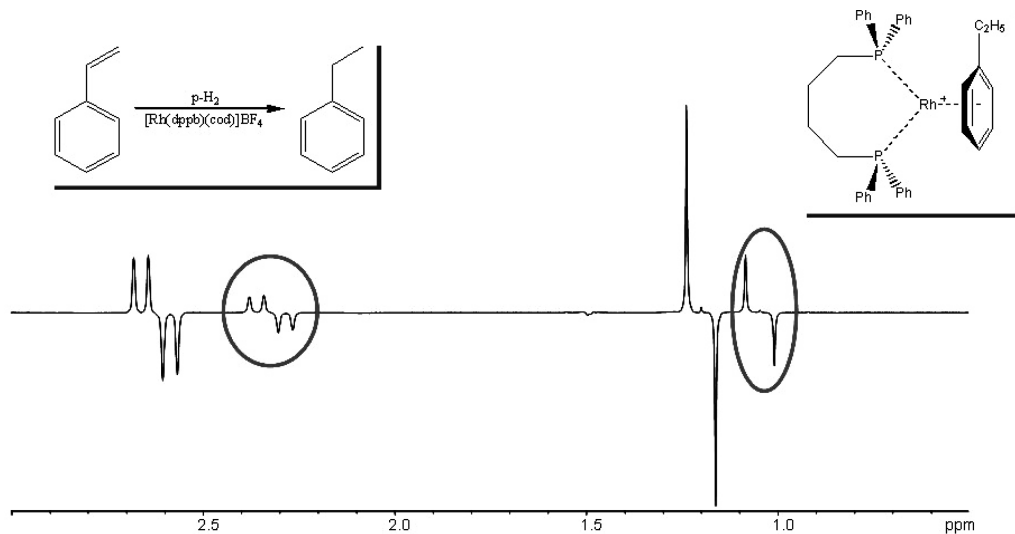


**Fig. 12.19** The  $^1\text{H}$ -PHIP-NMR spectrum and the anticipated intermediate product-catalyst- $\pi$ -complex observed during the hydrogenation of styrene.

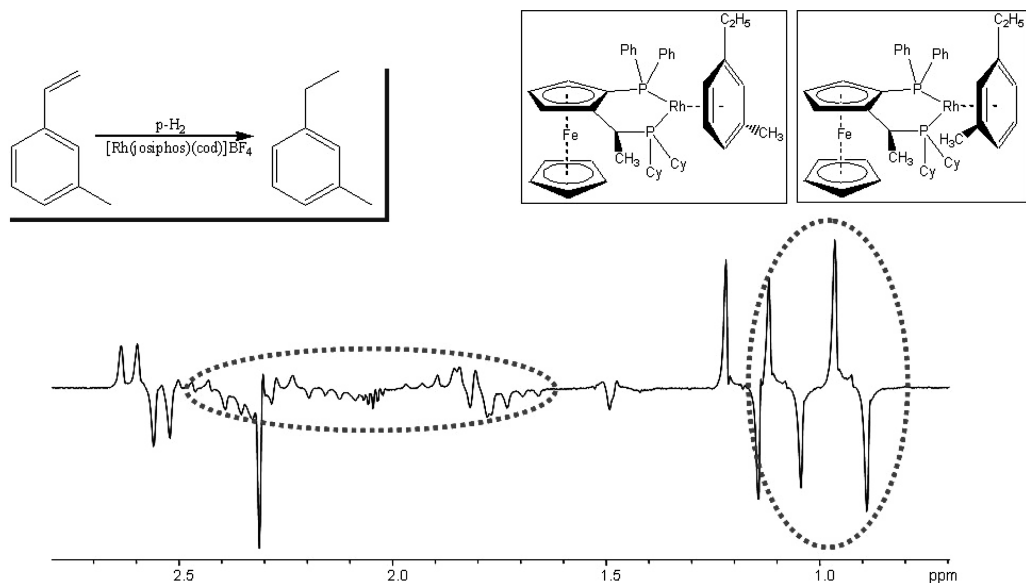


**Fig. 12.20** The  $^1\text{H}$ -PHIP-NMR spectrum and the anticipated two-intermediate product–catalyst–complexes observed during the hydrogenation of *meta*-methylstyrene.

#### 12.4.1

##### Enantioselective Substrates

If the substrate is enantioselective, as for example *meta*-methylstyrene, the “satellites” split into (at least) two separate resonances, respectively, for the  $\text{CH}_2$ - and the  $\text{CH}_3$ -resonances of the resulting product *meta*-methyl-ethylbenzene (Fig. 12.20).

#### 12.4.2

##### Chiral Catalysts

As opposed to the *meso* forms of catalyst, their chiral counterparts give rise to more complex  $^1\text{H}$ -PHIP-NMR spectra of the catalyst-attached intermediates. This fact is outlined for the selection of precatalysts and catalysts derived from those listed in Figure 12.21.

Figure 12.22 shows the  $\text{CH}_2$ -resonance of the catalyst-attached intermediates observed during the hydrogenation of styrene using an achiral catalyst, whilst Figure 12.23 depicts the same region of the spectrum of the intermediate when employing a chiral catalyst. In the latter case the more complex splitting pattern is clear. Finally, Figure 12.24 depicts the  $\text{CH}_2$ - and  $\text{CH}_3$ -resonances observed in the  $^1\text{H}$ -PHIP-NMR spectrum of the catalyst-attached intermediates observed during the hydrogenation of styrene, using the catalysts listed in Figure 12.21.



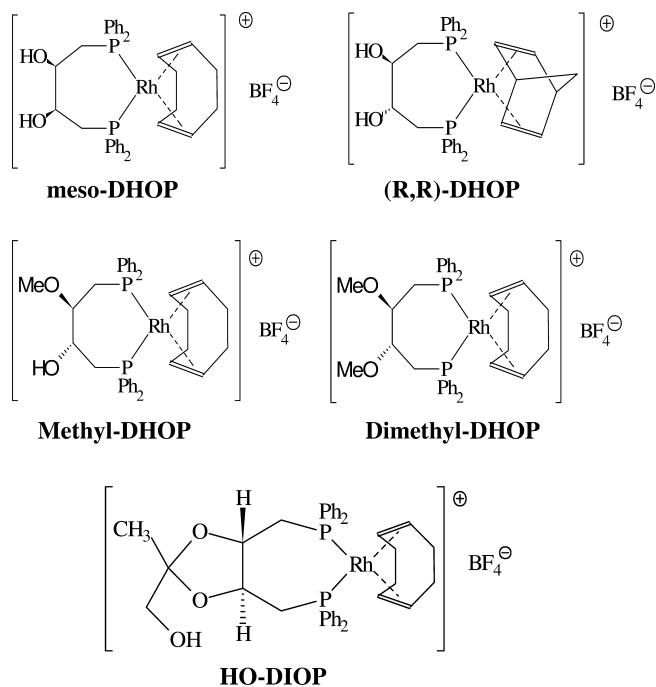


Fig. 12.21 Chiral and achiral Rh-catalysts employed for the hydrogenation of styrene.

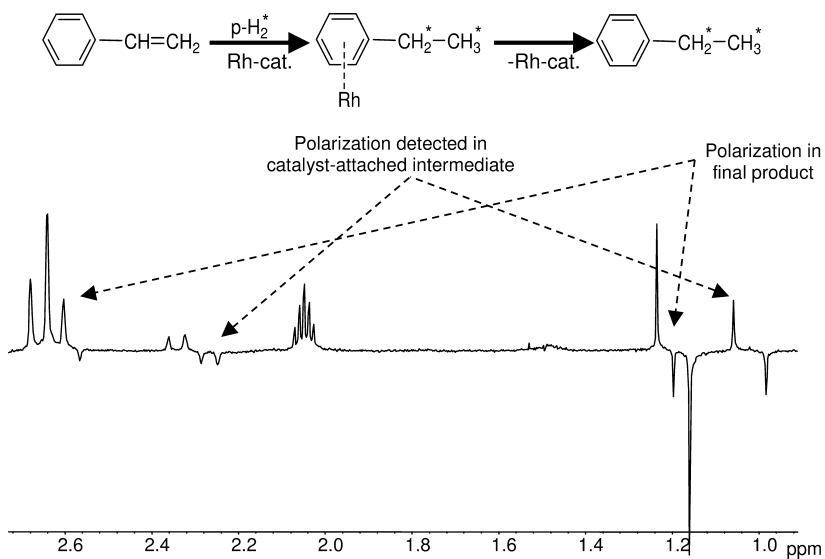
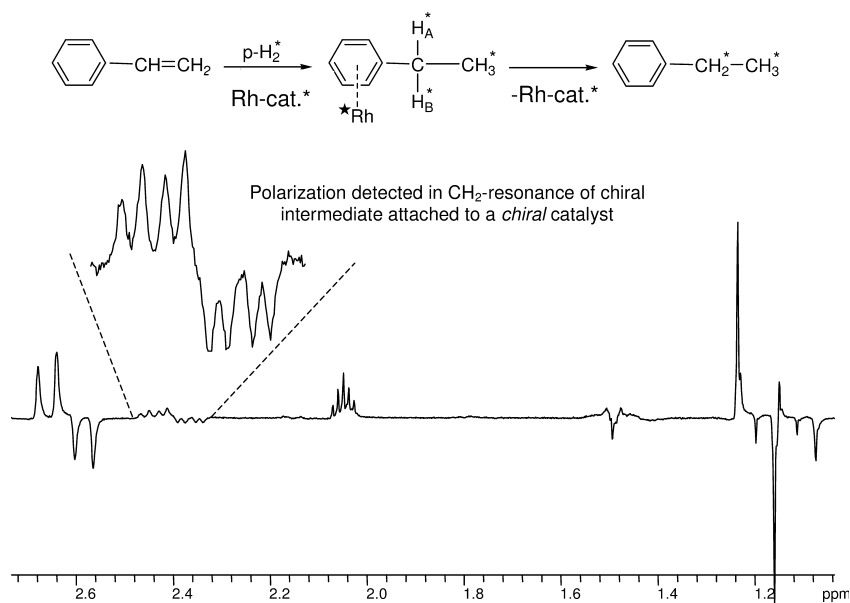


Fig. 12.22  $\text{CH}_2^*$ - and  $\text{CH}_3^*$ -resonances observed in the  $^1\text{H}$ -PHIP-NMR spectrum of the intermediate attached to an achiral catalyst during the hydrogenation of styrene.



**Fig. 12.23** CH<sub>2</sub>- and CH<sub>3</sub>-resonances observed in the <sup>1</sup>H-PHIP-NMR spectrum of the intermediate attached to a chiral catalyst during the hydrogenation of styrene.

### 12.4.3

#### Determination of Kinetic Constants

The formation and decay of these product–catalyst- $\pi$ -complexes are expected to occur according to the sequence of reactions as outlined in Scheme 12.4. The kinetic constants associated with the occurrence of  $k_{\text{HYD}}$  and the decay of  $k_{\text{OFF}}$ , respectively, can both be determined by PHIP-NMR using a process termed dynamic PASADENA (DYPAS) spectroscopy, as has been outlined previously [37]. For this purpose the addition of parahydrogen to the reaction is synchronized with the pulse sequences of the NMR spectrometer, whereby the time for acquiring the NMR spectra is delayed by variable amounts. The results thereof are listed in Table 12.3. A variety of kinetic constants can be determined, and the method is reasonably accurate; the margins of error are also indicated in Table 12.3 [37].

The data reveal that electron-donating groups such as amino- or alkoxy-groups increase the rate of formation of  $k_{\text{HYD}}$  according to their donor strength; for the rate of decay, such a correlation is more likely opposite – that is, they decrease the rate of decay of  $k_{\text{OFF}}$ . Similar observations have been made for electron-withdrawing substituents, which decrease the rate of formation of  $k_{\text{HYD}}$  according to their acceptor strength, but increase the rate of decay of  $k_{\text{OFF}}$ . Again, a free-energy correlation appears to be possible (unpublished results). One clear consequence of this correlation is a variable relative intensity of “satellite” resonances

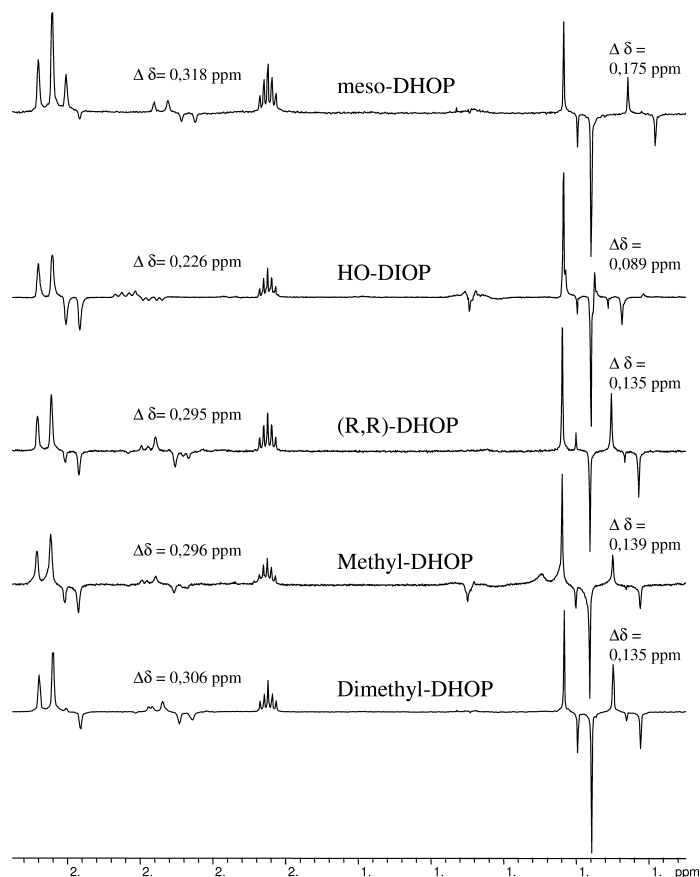
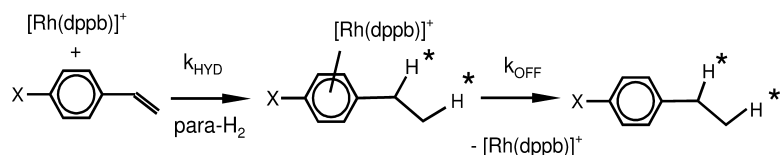


Fig. 12.24 CH<sub>2</sub>- and CH<sub>3</sub>-resonances observed in the <sup>1</sup>H-PHIP-NMR spectrum of the intermediate attached to the selection of various catalysts during the hydrogenation of styrene.



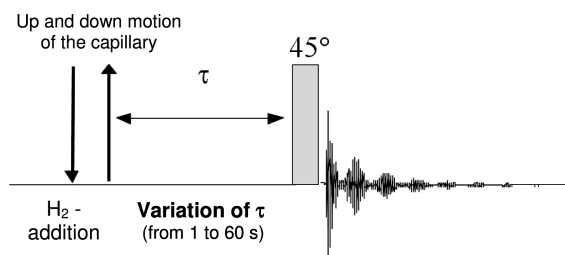
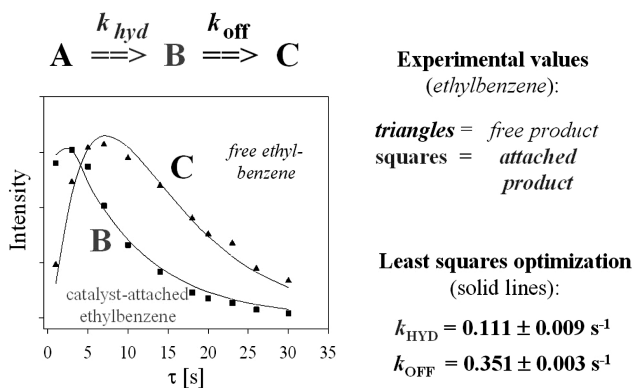
Scheme 12.4

and those of the final hydrogenation products. In cases where the rate of formation  $k_{\text{HYD}}$  is high, but the rate of decay of  $k_{\text{OFF}}$  is low, the intensity of the satellites can exceed those of the final hydrogenation products.

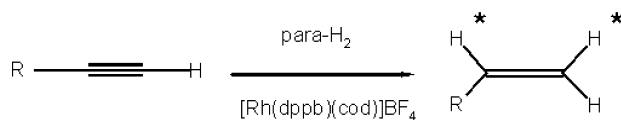
The principle of the DYPAS experiment is outlined in Figure 12.25. The results derived from the DYPAS experiments (see Table 12.3) of reactions following Scheme 12.4 may be represented pictorially as the time-dependence of the

**Table 12.3** Rates of formation and of decay of the interim product–catalyst- $\pi$ -complexes [44].

X-	$k_{\text{HYD}} [\text{s}^{-1}]$	$k_{\text{OFF}} [\text{s}^{-1}]$
-H	$0.111 \pm 0.009$	$0.35 \pm 0.03$
-OMe	$0.138 \pm 0.010$	$0.45 \pm 0.04$
-OEt	(0.40)	$0.273 \pm 0.024$
-NH <sub>2</sub>	(0.84)	$0.113 \pm 0.036$

**Fig. 12.25** The principle of the DYPAS experiment.**Fig. 12.26** Plots of the time-dependence of concentrations of the intermediates and products of the hydrogenation of styrene.

intermediate and the final product of two consecutive reactions (Fig. 12.26). Unlike the standard appearance of a plot of time-dependence of final product for two consecutive reactions, which typically shows asymptotic saturation behavior, the curve for the signal intensity of C also decays, due to relaxation of the PHIP-derived signal enhancement of this product. The DYPAS method is not restricted to the determination of the kinetic constants listed in Table 12.3, but may also be used to determine other rates of formation and decay (Table 12.4).



**Scheme 12.5** Hydrogenation of differently substituted ethynylbenzenes.

**Table 12.4** Rates of hydrogenation of differently substituted ethynylbenzenes.

Substrate	R-	$k_{\text{HYD}} [\text{s}^{-1}]$
1	Ph-	$0.140 \pm 0.005$
2	$(\text{CH}_3)_3\text{C}$ -	$0.085 \pm 0.002$
3	$(\text{CH}_3)\text{Si}$ -	$0.064 \pm 0.004$
4	$(\text{Ph})_3\text{Si}$ -	$0.085 \pm 0.003$

As a further example, the hydrogenation of differently substituted ethynylbenzenes have been investigated using the catalyst  $[\text{Rh}(\text{dppb})(\text{cod})]\text{BF}_4$ . The reaction is outlined in Scheme 12.5 and the results are listed in Table 12.4.

#### 12.4.4

##### Computer-Assisted Prediction and Analysis of the Polarization Patterns: DYPAS2

For *in-situ* studies of reaction mechanisms using parahydrogen it is desirable to compare experimentally recorded NMR spectra with those expected theoretically. Likewise, it is advantageous to know, how the individual intensities of the intermediates and reaction products depend on time. For this purpose a computer simulation program DYPAS2 [45] has been developed, which is based on the density matrix formalism using superoperators, implemented under the C++ class library GAMMA.

DYPAS2 [45] offers a large variety of simulation modes and allows the calculation of polarization patterns of the expected NMR spectra derived either from parahydrogen or orthodeuterium. Furthermore, the individual boundary conditions can be taken into account, under which the hydrogenations take place. Accordingly, the magnetic field dependence of the resulting polarization patterns can be predicted, for example in spectra based on the PASADENA or ALTADENA effect, respectively.

The kinetics of hydrogenation transfer is covered by the use of an exchange superoperator assuming a pseudo first-order reaction. Thereby, competing hydrogenations of the substrate to more than one product can also be accommodated. In addition, the consequences of relaxation effects or NOEs can be included into the simulations if desired. Furthermore, it is possible to simulate the consequences of different types of pulse sequences, such as PH-INEPT or INEPT+, which have previously been developed for the transfer of polarization from the parahydrogen-derived protons to heteronuclei such as  $^{13}\text{C}$  or  $^{15}\text{N}$ . The

individual delays required in these pulse sequences are critical parameters for the associated magnitude of the transferred polarization, but it is not trivial to estimate their optimal values. Therefore – and in particular for large spin systems – it is desirable to obtain access to intensity plots, which display the calculated intensities of the polarization-enhanced NMR spectra of the heteronuclei as a function of the individual delay times. DYPAS2 contains this option and provides an even greater variety of other possibilities [45].

## 12.5

### Colloidal Catalysts

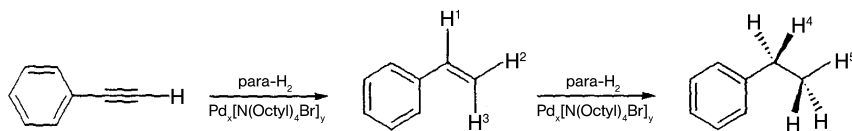
#### 12.5.1

#### *In-Situ* PHIP-NMR Investigation of the Hydrogenation of Ethynylbenzene by $\text{Pd}_x[\text{N}(\text{octyl})_4\text{Cl}]_y$

It is recognized that some colloidal catalysts show “homogeneous”-like behavior, though for the most part it is unclear which parameters define the borderline between heterogeneous- (i.e., surface reactions) and homogeneous-type catalysis of colloidal systems. The reaction of ethynylbenzene (phenylacetylene) with parahydrogen using the colloidal palladium catalyst  $\text{Pd}_x[\text{N}(\text{octyl})_4\text{Cl}]_y$  leads to nuclear spin polarization in the hydrogenation products [38]. Heterogeneous catalysts are not expected to give rise to the PHIP effect, as the spin correlation in the adsorbed  $p\text{-H}_2$  is considered to be lost once the dihydrogen molecules interact with a catalytically active surface. Therefore, most likely hydrogen atoms transferred in such fashion would stem from different  $p\text{-H}_2$  molecules. However, it has been shown that the colloidal transition-metal catalyst system  $\text{Pd}_x[\text{N}(\text{octyl})_4\text{Cl}]_y$  gives rise to the PHIP phenomenon, thereby implying a homogeneous reaction pathway and proving that the two transferred hydrogen atoms stem from the same dihydrogen molecule (Scheme 12.6).

For this purpose, standard 5-mm NMR tubes were charged with 100  $\mu\text{L}$  ethynylbenzene, 6 mg of the catalyst  $\text{Pd}_x[\text{N}(\text{octyl})_4\text{Cl}]_y$ , and 0.7 mL acetone- $d_6$  and placed into a 200-MHz spectrometer. Charges of 51%-enriched  $p\text{-H}_2$  were prepared as previously outlined via catalytic equilibration over charcoal at 77 K and injected repeatedly in synchronization with the pulsed NMR-experiment via an electromechanically lowered glass capillary mechanism.

The PHIP-NMR spectra shown in Figure 12.27 were obtained during the hydrogenation of 4-chlorostyrene with  $p\text{-H}_2$  parahydrogen [38]. In order to elimi-



**Scheme 12.6** Hydrogenation of phenylacetylene using a colloidal Pd-catalyst system.

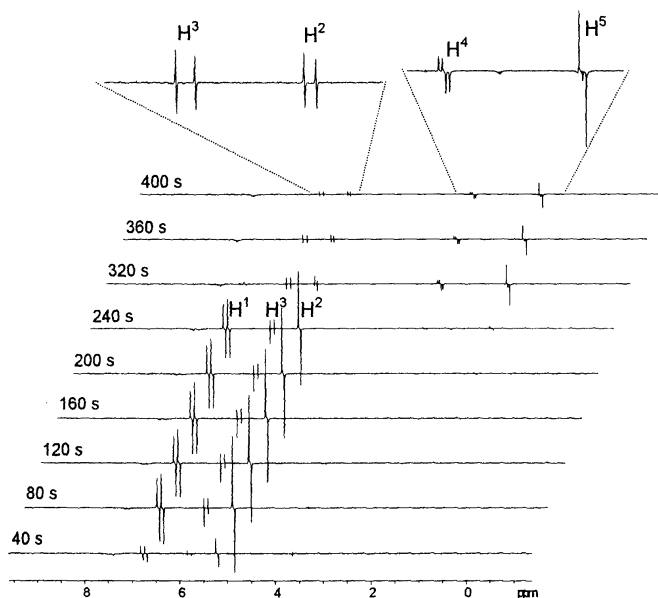


Fig. 12.27 200 MHz  $^1\text{H}$ -PHIP-NMR spectra recorded during the hydrogenation of phenylacetylene using a colloidal Pd catalyst.

nate interfering signals originating from spins in thermal equilibrium (i.e., “non-PHIP signals”), the NMR spectra were acquired after a hydrogenation time of 10 s accumulating the responses to different pulse angles.

The maximum signal intensity for  $^1\text{H}$ -PHIP signals occurs at a flip angle of  $45^\circ$ , in contrast to the usual “ $90^\circ$  pulse” used for substrates in thermal equilibrium. Therefore, by alternately adding and subtracting scans acquired using pulse angles of  $-45^\circ$  and  $135^\circ$ , respectively, it is possible to minimize or even suppress the signal intensity of the “unpolarized”, so-called “thermal” proton spins, whereas the signals of the proton spins in polarization then display the maximum of their signal intensity. Less than perfect elimination of the thermal signals may occur, nevertheless, in part because of a slight drift of the external magnetic field ( $B_0$ ), or because of changes of the homogeneity. Each spectrum shown in Figure 12.27 is the result of four accumulated scans and 40 s of hydrogenation time each.

*Cis* hydrogenation of ethynylbenzene leads to polarization signals in the respective positions  $\text{H}^1$  and  $\text{H}^2$  of styrene (Scheme 12.6), as is detected. Furthermore, polarization also occurs in position  $\text{H}^3$ . This signal shows an anti-phase coupling of 1 Hz with its geminal hydrogen. In order to distinguish whether this is a result of geminal transfer of  $p\text{-H}_2$  parahydrogen to the positions  $\text{H}^2$  and  $\text{H}^3$ , or the consequence of a NOE, the use of deuterated ethynylbenzene is required.

With proceeding hydrogenation, the concentration of ethynylbenzene decreases; therefore, the positions  $\text{H}^1$  and  $\text{H}^2$  show increasingly less polarization.

Subsequently, the polarization signals  $H^4$  and  $H^5$  of ethylbenzene (i.e., the hydrogenation product of styrene) appear. Accordingly, ethylbenzene is also formed via homogeneous catalysis as well – that is, two more  $p\text{-H}_2$  protons are transferred simultaneously.

The hydrogenation of ethynylbenzene to styrene (as well as that of styrene to ethylbenzene) mediated by the colloidal catalyst  $\text{Pd}_x[\text{N}(\text{octyl})_4\text{Cl}]_y$  occurs in a “pair-wise” fashion – that is, the two hydrogen atoms of dihydrogen are transferred simultaneously, which is otherwise characteristic of a homogeneous hydrogenation. This *in-situ* NMR experiment convincingly demonstrates the unique power of PHIP for the investigation of hydrogenations mediated by colloidal systems.

## 12.6

### Transfer of Proton Polarization to Heteronuclei

#### 12.6.1

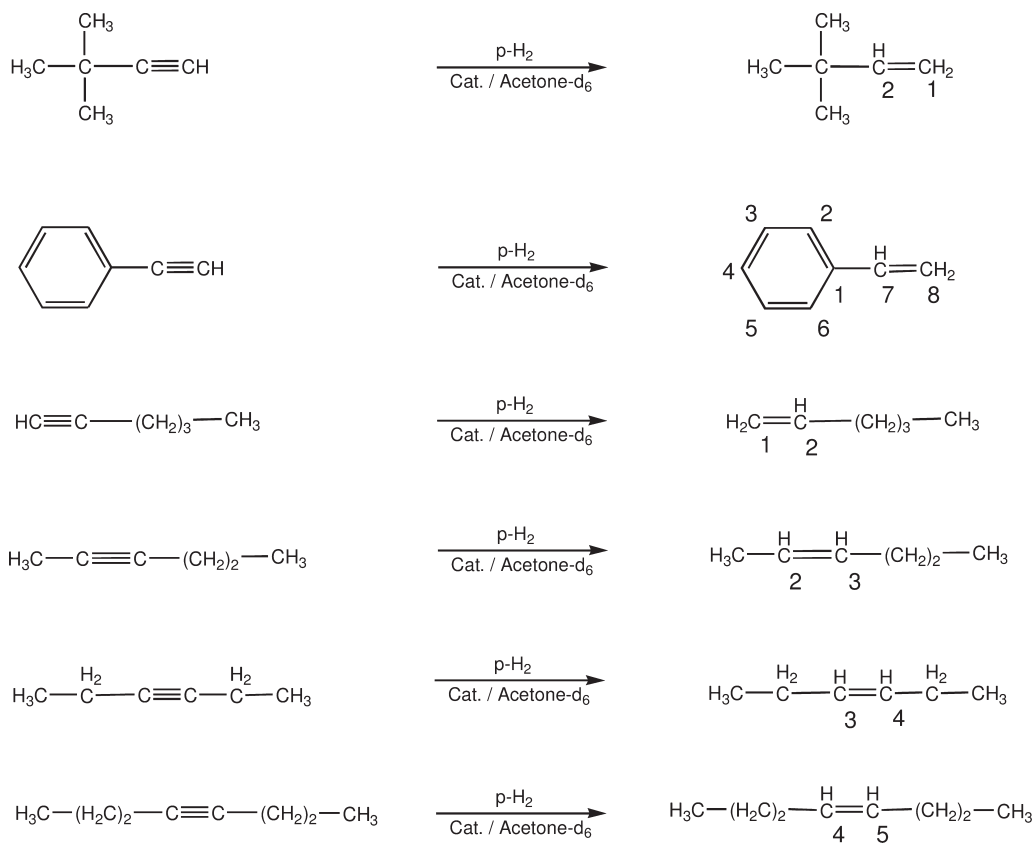
##### General Aspects

Homogeneously catalyzed hydrogenations of unsaturated substrates with parahydrogen leading to strong polarization signals in  $^1\text{H}$ -NMR spectra also give rise to strong heteronuclear polarization, especially if the hydrogenations are carried out at low magnetic fields. The mechanisms underlying the process of PHIP transfer to heteronuclei, however, are still not fully understood, and different mechanisms have been discussed. The polarization transfer from protons to carbon nuclei during the hydrogenation of alkynes may serve as a typical example, which has been investigated for several substrates. It could be shown that in systems containing easily accessible triple bonds (Table 12.5) (e.g., ethynylbenzene or 2,2-dimethylbutyne), a polarization transfer takes place to all carbon nuclei in the molecule. Accordingly, all  $^{13}\text{C}$  resonances can be observed in NMR spectra recorded *in situ* with good to excellent signal-to-noise ratios (SNRs) using only a single transient [42]. This technique has made it possible to identify a Ru-based catalyst system, which yields *E*-alkenes via homogeneous hydrogenations of alkynes with central triple bonds, as opposed to the more conventional *Z*-alkenes that result from hydrogenation with Rh-based catalysts [47].

PHIP studies together with polarization transfer permit elucidation of the structure (i.e., the carbon skeleton of compounds) in a fashion which is far superior to the conventional  $^1\text{H}$ -PHIP technique outlined above.

Furthermore, the qualitative influence of substituents on the symmetry and electronic structure of the substrate and its hydrogenation product on the efficiency of the transfer of polarization to the  $^{13}\text{C}$ -nuclei have been discussed, as well as the feasibility of a polarization transfer to other heteronuclei. Evidence in the form of a shift of the aromatic  $^{13}\text{C}$  resonances has been found for an initial attachment of hydrogenation products containing aromatic segments to the metal center of the cationic hydrogenation catalyst – probably in the form of a  $\pi$ -complex.



**Table 12.5** Reactions studied using  $^{13}\text{C}$ -PHIP-NMR spectroscopy.

It has been postulated [39] and demonstrated previously that “Hetero-PHIP” for nuclei such as  $^{13}\text{C}$ ,  $^{29}\text{Si}$ , and  $^{31}\text{P}$  can result in a signal enhancement (SE)  $>10$  [8, 40, 41], particularly if the reactions are carried out at low magnetic fields (i.e., under ALTADENA conditions).  $^{31}\text{P}$  INEPT(+ $\pi/4$ ) experiments have also been carried out to transfer the initial proton polarization to  $^{31}\text{P}$  [8].

Barkemeyer et al. [8a] showed previously that high enhancement can also be achieved at high magnetic fields when hydrogenating symmetric systems, where the breakdown of symmetry is caused by the naturally abundant  $^{13}\text{C}$  nuclei occurring individually in the two other equivalent carbon atoms of the double bond of the substrate (see Scheme 12.8) [8a].

Although this phenomenon provides a powerful tool for the NMR investigation of low- $\gamma$  nuclei, the full potential of this sizeable polarization transfer from parahydrogen to other nuclei has not been applied very much as compared to  $^1\text{H}$ -PHIP-NMR spectroscopy. In particular, the use of the PHIP effect to en-

hance and correspondingly simplify the detection of carbon nuclei is a powerful tool for investigating the structure of organic molecules.

### 12.6.2

#### Polarization Transfer to $^{13}\text{C}$

The PHIP phenomenon may be used to label specifically individual, naturally occurring  $^{13}\text{C}$  nuclei magnetically via specific enhancement of their corresponding resonances. This frequently simplifies the assignment, thereby facilitating the interpretation of  $^{13}\text{C}$ -NMR spectra of more complex molecules. The polarization phenomena occurring in the  $^{13}\text{C}$ -PHIP-NMR spectra during the *in-situ* hydrogenation of various alkynes using the catalyst  $[\text{Rh}(\text{cod})(\text{dppb})]^+$  in  $\text{CDCl}_3$  at 5 bar of parahydrogen may serve as a characteristic example [42].

The spectra depicted in Figure 12.28 were recorded during the hydrogenation of 3,3-dimethylbut-1-yne to 3,3-dimethylbut-1-ene, and occur according to Scheme 12.7. As is apparent from Figure 12.28, signals from all carbon atoms are visible and nearly all expected couplings can be determined accordingly.

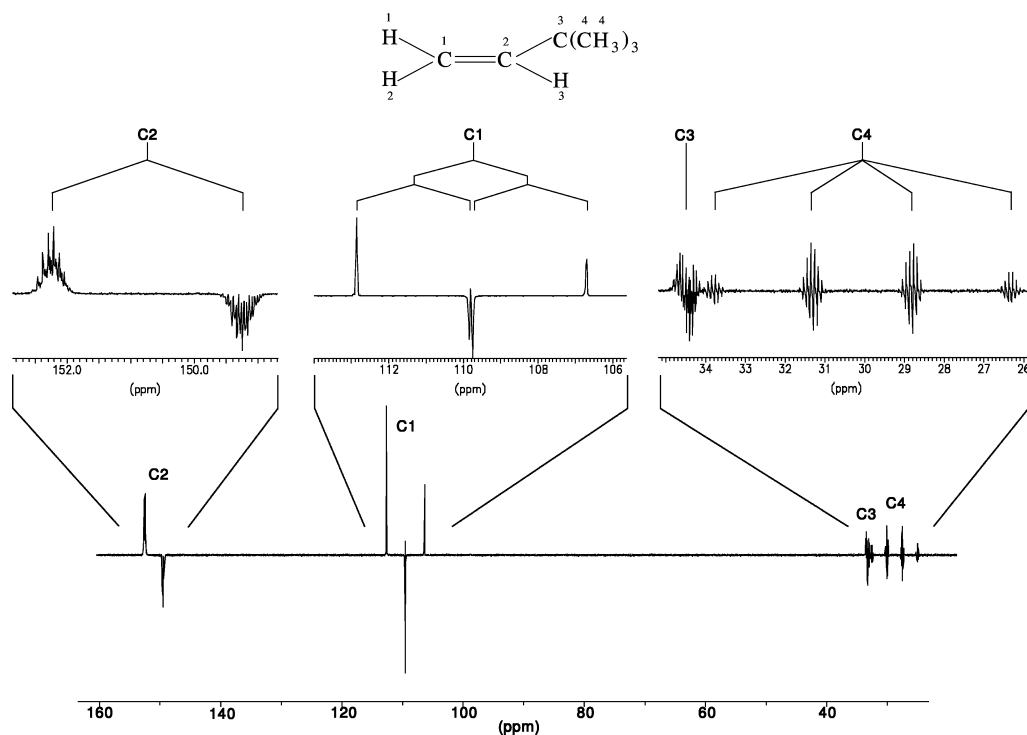
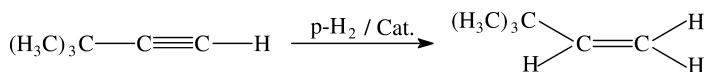


**Fig. 12.28**  $^{13}\text{C}$ -PHIP spectrum of the hydrogenation of 3,3-dimethylbut-1-yne to 3,3-dimethylbut-1-ene.



**Scheme 12.7** Hydrogenation of 3,3-dimethylbut-1-yne to 3,3-dimethylbut-1-ene.

Other alkynes investigated include ethynylbenzene, 1-hexyne, 2-hexyne, 3-hexyne, and 4-octyne (Table 12.5). These substrates have in common that the triple bond is rather accessible. The substituents cover a wide range of different electronic structures and steric requirements, and in addition, they provide for symmetric and asymmetric substrates. Within this selection of hexynes the electronic structure and accessibility of the individual triple bonds are almost the same, but the symmetry of the bond is different. Furthermore, 1-hexyne, 3,3-dimethylbutyne, and ethynylbenzene all have terminal triple bonds, but the electronic structure and accessibility of the  $\pi$ -system of these triple bonds are influenced differently by the catalyst, depending on the group adjacent to the triple bond. Within this series it could be shown how +M and +I effects or steric hindrance influence the hydrogenation and polarization transfer from the protons to the carbon atoms [42]. The six reactions investigated are outlined in Table 12.5 – that is, the starting materials and the corresponding reaction products, together with the numeration of the individual carbon atoms following IUPAC nomenclature.

The corresponding signal enhancements, as well as the magnitude of the polarization transfer from the former parahydrogen atoms to the directly adjacent former acetylenic carbon, and also to other carbon atoms in the product molecules, have been compared, whereby the polarization spectra were measured under ALTADENA conditions. This means that the hydrogenation was conducted within the Earth's magnetic field, upon which the reaction solution was transferred into the high magnetic field of the superconducting magnet of the NMR spectrometer (corresponding to a proton resonance frequency of 200 MHz or  $\sim 50$  MHz for the  $^{13}\text{C}$  nuclei, respectively) to detect the PHIP spectra. By means of this procedure, polarization is transferred to all magnetically active nuclei in the following way. The resonance frequencies of all nuclei in this very low magnetic field of the Earth (or less) are all virtually the same. Therefore, a highly coupled spin system of a high order is obtained – that is, the differences of resonance frequencies between the carbons ( $^{13}\text{C}$ ) and the protons are small compared to their coupling constants. This is essential for the polarization transfer from protons to a large number of carbons.

By contrast, in the high field of a superconducting magnet, polarization transfer to heteronuclei is less efficient, because now the difference in resonance frequency of  $^1\text{H}$  and  $^{13}\text{C}$  is significant and exceeds the magnitude of the coupling constants between the carbons and the protons. In this latter case, polarization transfer can be achieved most effectively by appropriate pulse sequences (e.g., via cross-polarization).

For these experiments, standard 5-mm NMR tubes equipped with a screw cap and a septum were charged with 200  $\mu\text{L}$  of the substrate, 6 mg of the catalyst  $[\text{Rh}(\text{cod})(\text{dppb})]\text{BF}_4$  (Cat.), 0.7 mL of degassed chloroform- $\text{d}_1$ , and 5 bar of 50%-

enriched parahydrogen. This degree of enrichment was achieved via catalytic equilibration over charcoal at 77 K. Higher levels of enrichment, namely >97%, have also been achieved using a closed-cycle cooler cryostat.

In this fashion,  $^{13}\text{C}$ -PHIP-NMR spectra were obtained using the six substrates 3,3-dimethylbut-1-yne, ethynylbenzene, 1-hexyne, 2-hexyne, 3-hexyne, and 4-octyne, respectively. The relevant spectroscopic data for these substrates were obtained from a database [43]. All  $^{13}\text{C}$  spectra could be recorded using only a single transient, as they exhibited a higher SNR than expected. The enhanced SNR is due to the PHIP effect, and results from a transfer of the initial proton polarization of the parahydrogen to the carbon atoms. Because of the strong signal enhancement caused by the PHIP effect, no signals were visible for the carbon atoms of the starting material. In general, it is not possible to obtain carbon spectra using just a single transient, at least not with such a high SNR.

Normally in  $^{13}\text{C}$ -NMR spectra, the solvent gives rise to the strongest signal of the spectrum; therefore, it frequently must be suppressed via an appropriate pulse sequence. In  $^{13}\text{C}$ -PHIP-NMR spectroscopy as outlined here, however, this is not necessary; rather, the signal due to the solvent  $\text{CDCl}_3$  (normally occurring as a triplet at  $\delta=77.7$  ppm) is not even visible, at least not in the more favorable cases. In all reactions investigated, the signals of all carbon atoms in the products could be detected exploiting only a single transient, which yields a good to excellent SNR.

Although a polarization transfer to all carbon atoms in the corresponding substrates is observed universally, the associated SNR is quite different for the individual substrates. By contrast to the  $^1\text{H}$ -PHIP-NMR spectra, namely, the  $^{13}\text{C}$ -PHIP-NMR spectra observed exhibit much more significant differences depending on the individual substrates. In general, in the  $^1\text{H}$ -NMR the SNR is much higher; therefore, small differences cannot be distinguished so easily, whereas for  $^{13}\text{C}$ -NMR and accordingly for  $^{13}\text{C}$ -PHIP-NMR this is much easier. In addition, in  $^1\text{H}$ -PHIP-NMR the polarization is only transferred to the adjacent protons not further away than approximately corresponding to a  $^3\text{J}$  coupling. For  $^{13}\text{C}$ , however, transfers of the polarization to carbon nuclei as far away as six bonds have been detected.

It is worthwhile pointing out that it is desirable to acquire all spectra under identical conditions, such as hydrogen pressure, elapsed time prior to the acquisition of the spectrum, temperature, and amount of catalyst used. For this reason it is desirable to use a set-up which permits the spectra to be recorded in totally standardized fashion, which does not depend on any individual "human factor". Such a system would allow the reaction to be conducted at a low magnetic field and would thereafter transfer the solution automatically (notably quickly and "adiabatically") into the NMR spectrometer for subsequent analysis.

In addition to the transfer of some degree of polarization to all carbon atoms in the product molecule, a slight low field shift of the  $^{13}\text{C}$  resonances in the aromatic region of the PHIP-NMR spectrum of the product recorded during the hydrogenation of ethynylbenzene can be observed. A similar effect has been observed before in the  $^1\text{H}$ -PHIP-NMR spectra recorded during the hydrogenation of styrene derivatives using cationic rhodium catalysts. This phenomenon has

been termed “product attachment” (see Section 12.4), implying that the hydrogenation product binds to the catalyst’s metal center via the phenyl ring in the form of a  $\pi$ -complex. The strength of this attachment depends on the electronic structure of the product and the catalyst, and it can either lead to a shift to high or low frequencies in the  $^1\text{H}$ -NMR spectrum. By contrast to the  $^1\text{H}$ -PHIP-NMR investigations of this product attachment (as reported earlier), the effect as observed here in  $^{13}\text{C}$ -PHIP-NMR spectra is more pronounced. For  $^1\text{H}$ -NMR the magnitude of this shift is about 0.5 ppm, whereas for  $^{13}\text{C}$ -NMR a shift of about 4 ppm was observed. However, considering the wider range of  $^{13}\text{C}$ -shifts compared to those of  $^1\text{H}$ -nuclei, this is to be expected.

These  $^{13}\text{C}$ -PHIP-NMR investigations show clearly that it is possible to effectively transfer polarization from parahydrogen to  $^{13}\text{C}$  atoms, especially when conducting the hydrogenations at low magnetic fields. This polarization transfer clearly depends on the electronic and steric features of the groups adjacent to the triple bond. The strongest  $^{13}\text{C}$ -PHIP-NMR signals have been observed using either 3,3-dimethylbutyne or ethynylbenzene as the substrate, whereby a transfer of the polarization has been observed for all carbon atoms in the molecule, associated with an excellent SNR. Furthermore, the hydrogenation of 1-hexyne also shows polarization and signal enhancement for all carbon nuclei, but the SNR is not as good as it is for 3,3-dimethylbutyne or ethynylbenzene. With 2-hexyne as the substrate, polarization transfer is observed for all carbon nuclei likewise. Finally, during the hydrogenation of 3-hexyne to 3-hexene, and of 4-octyne to 4-octene, respectively, polarization signals are also observed, with good intensity for the two carbons of the olefinic group and of all aliphatic carbon nuclei. This is consistent with previous studies of other symmetrically substituted alkynes showing strong  $^{13}\text{C}$ -PHIP-NMR signals, and it is especially true for symmetrically substituted alkynes carrying electron-poor substituents (e.g., acetylene dicarboxylic acid and its esters). This finding has now been extended to electron-rich alkyne substrates.

When acquiring NMR spectra under ALTADENA conditions, polarization is transferred to all magnetically active nuclei in the substrate. This means that the initial polarization of the parahydrogen is distributed over the number of atoms present in the substrate. This “sharing of the polarization” permits an explanation of the observed decrease in intensity from 3,3-dimethylbut-1-yne or ethynylbenzene to the hexynes, and 4-octyne. In the latter two cases there are more nuclei participating in this sharing. Additionally, the good accessibility of the terminal triple bond of 3,3-dimethylbut-1-yne, ethynylbenzene, and 1-hexyne implies an easy hydrogenation of these substrates, yielding a higher SNR in contrast to the SNR of 2- and 3-hexyne carrying a more central and hence less-accessible triple bond. Finally, the electron-richness of 3,3-dimethylbut-1-yne or ethynylbenzene facilitates the coordination of these substrates to the metal center of the catalyst, thereby resulting in a slightly better SNR, than is the case for 1-hexyne.

Because of the low natural abundance of  $^{13}\text{C}$  nuclei (1.1%), practically all observed product molecules contain only one  $^{13}\text{C}$  nucleus. Accordingly, the polarization signals in the  $^{13}\text{C}$  NMR spectrum clearly do not originate from one and

the same product molecule, but rather stem from different, singly labeled molecules. Since the fraction of the product molecules that contain two or even more  $^{13}\text{C}$  nuclei are practically negligible, the observed  $^{13}\text{C}$ -NMR spectra are the result of a superimposition of the spectra stemming from product molecules which contain only a single  $^{13}\text{C}$  nucleus at the respective position. Therefore, a transfer of polarization from the former parahydrogen atoms to an individual  $^{13}\text{C}$  nucleus cannot occur via transfer along the backbone (i.e., not along the carbon chain of the molecules), but it is caused by direct or indirect coupling, either scalar or dipolar, between the former parahydrogen nuclei, other protons, and the corresponding  $^{13}\text{C}$  nucleus.

In these experiments it was shown possible to transfer polarization, induced by the PHIP effect, to almost any given carbon in the hydrogenation product of an alkyne, and that certain asymmetrical and electronically activated substrates give rise to the strongest polarization transfer to  $^{13}\text{C}$  nuclei. In the cases of 3,3-dimethylbutyne or ethynylbenzene, all carbon atoms were detected using only a single transient, and thereby yielding an excellent SNR [42]. Even with substrates that yield only a weaker polarization transfer (i.e., 1-, 2-, 3-hexyne, and 4-octyne) the SNR was significantly better than was obtained using conventional  $^{13}\text{C}$ -NMR without accumulation. In favorable cases, the normally dominating  $^{13}\text{C}$  signals of the solvent (e.g.,  $\text{CDCl}_3$ ) are barely visible in the PHIP-enhanced spectra.

Because of large coupling constants between  $^{13}\text{C}$  and  $^1\text{H}$  (as compared to the coupling constants between  $^1\text{H}$  nuclei), polarization transfer to  $^{13}\text{C}$  nuclei is more effective than among protons. It appears that the maximum distance for transfer of polarization between protons (i.e., in  $^1\text{H}$ -PHIP-NMR) is about three bonds, whereas it is five for  $^{13}\text{C}$ -PHIP-NMR.

In addition to the observed polarization transfer, attachment of the hydrogenated product to the catalyst – most likely in the form of a  $\pi$ -complex between the aromatic portion of a product and the cationic catalyst – has also been observed in the  $^{13}\text{C}$ -PHIP-NMR spectra. The associated larger shift range of the affected  $^{13}\text{C}$  will make it possible to characterize the nature of this attachment as well as the associated binding energies of the hydrogenation product to the catalyst's metal center more precisely and effectively.

Figure 12.29 illustrates the  $^{13}\text{C}$ -PHIP spectrum obtained when hydrogenating 4-fluoro-1-ethynylbenzene under ALTADENA conditions in the Earth's magnetic field. The reaction proceeds according to Scheme 12.5 and the catalyst used is outlined there. This system and the other isomers thereof, namely the hydrogenation of 2-, 3-, and 4-fluoro-1-ethynylbenzene, have also been studied using  $^1\text{H}$ - and  $^{19}\text{F}$ -PHIP-NMR, and the results of the latter will be outlined in the following section (Fig. 12.30).

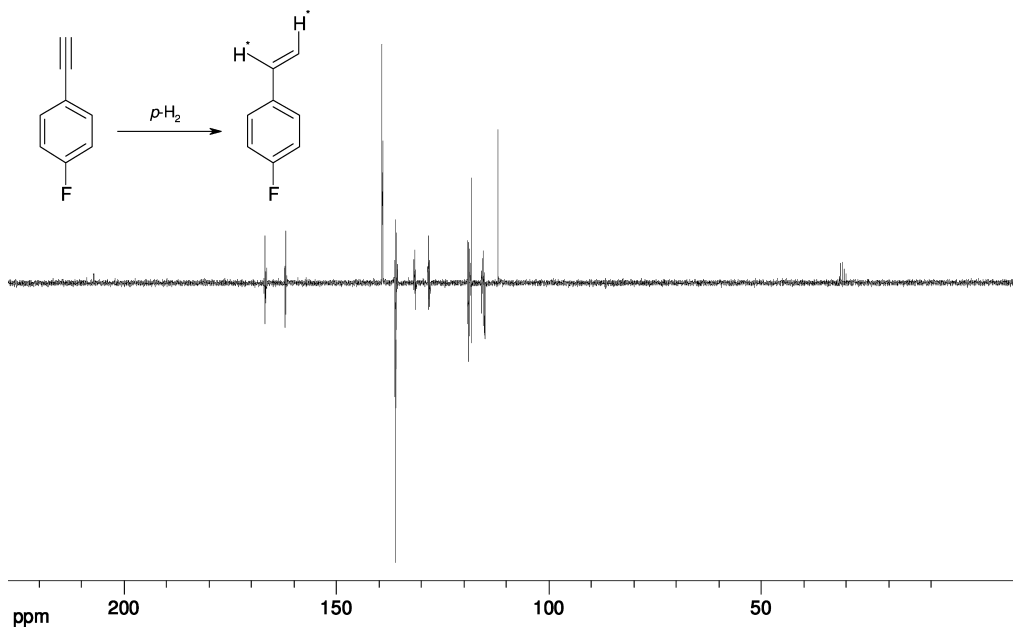


Fig. 12.29  $^{13}\text{C}$ -PHIP spectrum of the hydrogenation of 4-fluoro-1-ethynylbenzene.

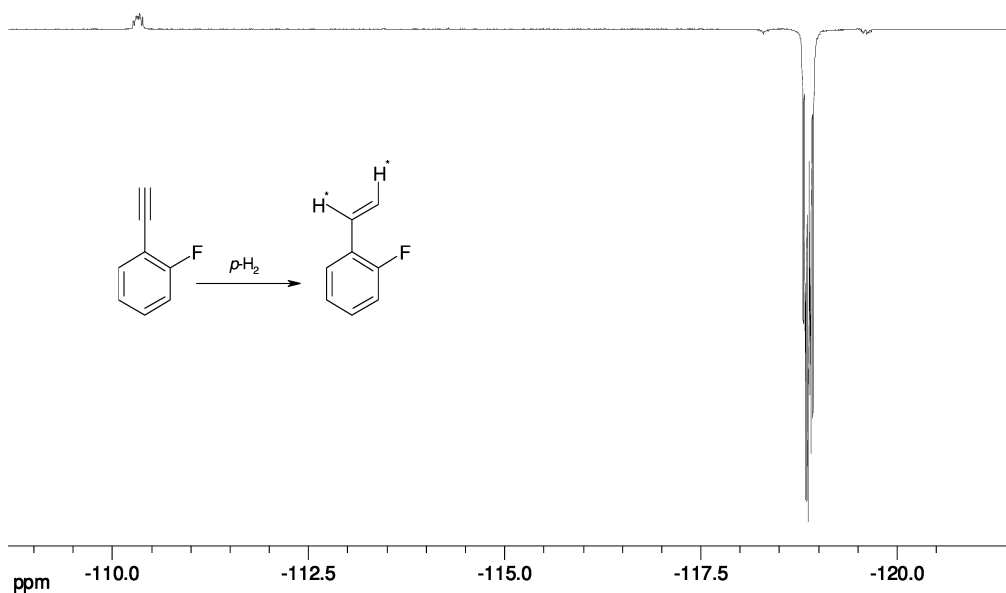


Fig. 12.30 ALTADENA- $^{19}\text{F}$ -PHIP-spectrum of the hydrogenation of 2-fluoro-1-ethynylbenzene.

## 12.6.3

**Polarization Transfer to  $^{19}\text{F}$** 

Transfer of the initial proton polarization is not confined to other protons or  $^{13}\text{C}$ , but the signals of other heteronuclei ( $^2\text{H}$ ,  $^{15}\text{N}$ ,  $^{29}\text{Si}$ ,  $^{31}\text{P}$ ) in the hydrogenation products can also become substantially enhanced, thereby also increasing their receptivity. Accordingly, the transfer of the PHIP-derived high spin order to  $^{19}\text{F}$  has been accomplished using a set of chemically similar fluorinated styrene and ethynylbenzene derivatives.

Additionally, the transfer to  $^{19}\text{F}$  occurs not only when the hydrogenation is initiated in the Earth's magnetic field (ALTADENA condition) but also when the whole reaction is carried out in the presence of the strong field of the NMR spectrometer (PASADENA). Both through-bond and through-space interactions are responsible for this process, termed parahydrogen-aided resonance transfer (PART). The high-field and low-field PHIP transfer mechanisms must be strictly distinguished, because they give rise to different phenomena [48].

The best results are obtained when using substrates associated with high hydrogenation rates and long spin-lattice relaxation time for all nuclei of interest, and if the reactions are carried out in the absence of the strong field of the NMR spectrometer. Therefore, in order to study the consequences of polarization transfer to  $^{19}\text{F}$ , the hydrogenations of  $^{19}\text{F}$ -containing ethynylbenzenes and

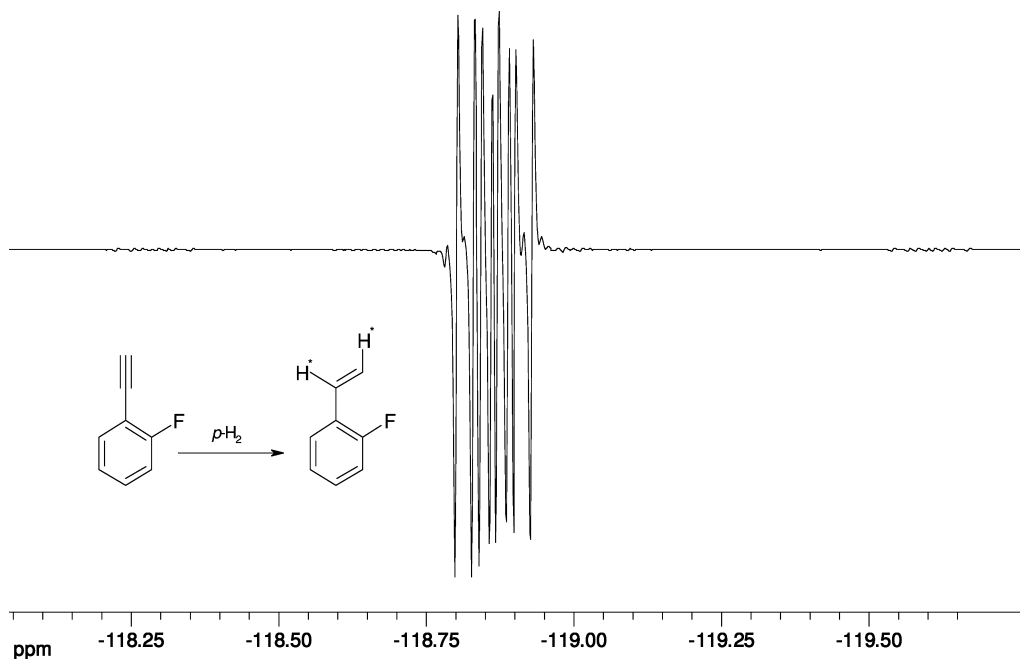
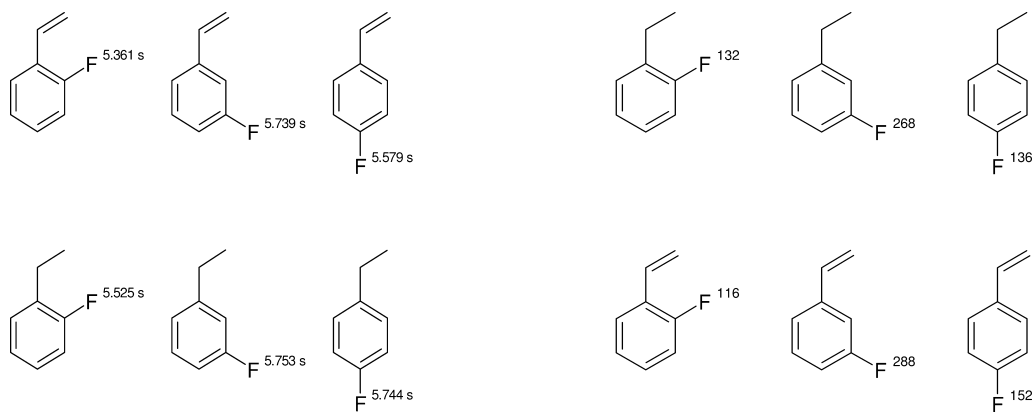


Fig. 12.31 PASADENA- $^{19}\text{F}$ -PHIP of the hydrogenation of 2-fluoro-1-ethynylbenzene.





**Fig. 12.32**  $^{19}\text{F}$ -NMR  $T_1$ -spin relaxation times (left) and  $^{19}\text{F}$ -PHIP ALTADENA enhancement factors (right) for the hydrogenation products shown.

styrenes have been investigated. It might be expected that if the chemical reaction occurred at high field (i.e., within a MRI or NMR magnet), the signal enhancement would be confined to certain protons only. Instead, if the reaction occurs at low field, the polarization might be transferred to heteronuclei such as  $^{31}\text{P}$ ,  $^{13}\text{C}$ , or  $^{19}\text{F}$ , without requiring any special pulse sequences. It transpires, however, that in these systems the  $^{19}\text{F}$  nuclei become spin polarized both at low field (Fig. 12.30) and at high field (Fig. 12.31), which opens up new possibilities.

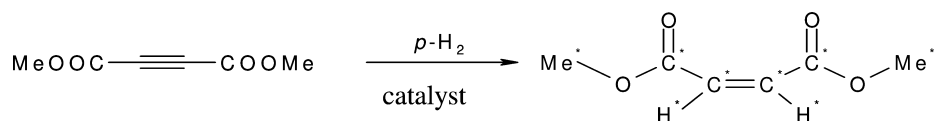
The pentafluorophenyl derivatives are particularly revealing, since the polarization transferred to the individual  $^{19}\text{F}$  positions can be compared and correlated with different concepts of their interactions with the primarily spin polarized protons [48]. The enhancement factors achieved in the hydrogenation products of monosubstituted compounds at low field under ALTADENA conditions are given in Figure 12.32.

Likewise, the initial proton polarization may be transferred to other magnetically active heteronuclei, most attractively to those associated with a low  $\gamma$ -value of their nucleus (i.e., to  $^{15}\text{N}$ ,  $^{29}\text{Si}$ ), and similarly “difficult” ones, using heteroatom PHIP at low magnetic fields [8, 45].

#### 12.6.4

##### Parahydrogen-Assisted Signal Enhancement for Magnetic Resonance Imaging

The initial observation of a significant PHIP-derived enhancement factor of  $>2500$  for  $^{13}\text{C}$  has rendered this approach attractive for heteronuclear magnetic resonance imaging (MRI) [49]. Using the system as outlined in Scheme 12.8 that is associated with an enhancement factor for  $^{13}\text{C}$  of 2500 [8 a], Golman et al. [49] have demonstrated the feasibility of heteronuclear MRI originally in the form of  $^{13}\text{C}$  angiography investigations.



**Scheme 12.8** Hydrogenation of acetylene dicarboxylic acid dimethyl ester to the corresponding maleate [8 a].

This initial system, though not optimized for this particular application in medicine, has since been superseded by more appropriate systems with other choices of the components [48]. Finally, possible applications for using selectively hyperpolarized fluorine-containing molecules as contrast agents for medical imaging techniques appear especially attractive; however, this subject matter is discussed elsewhere [50].

## 12.7

### Catalysts Containing other Transition Metals

Over the years, a considerable number of systems have been investigated, comprising catalysts that contain a variety of transition metals, including Co [5], Pd [59, 60], Pt [60, 61], Ru [47, 62], and Ta [63], although the most detailed studies have been conducted on systems containing either Rh or Ir (including some rather exotic ones [64]) as the transition metals. Even investigations on the surfaces of ZnO have been conducted successfully [59]. Further details have also been reported in earlier reviews [12 d, 34 c, 65].

## 12.8

### Summary and Conclusions

PHIP-NMR spectroscopy is an *in-situ* method, which is associated with a significant signal enhancement of both the protons as well as of various heteronuclei. On the basis of an associated increase in sensitivity, this approach and method allows the identification of unstable intermediates and previously elusive minor reaction products of homogeneous hydrogenations and other reactions. It brings about strong signal enhancement (factor  $\cong 1000$  for protons and even higher for heteronuclei such as  $^{13}\text{C}$ ). This increase in sensitivity renders it possible to detect and analyze crucial reaction intermediates. Therefore, structural and geometric conclusions can be made, and even the rate of formation and of the decay of the intermediates can be determined. The initial proton polarization can be transferred to heteronuclei and to yield enhancement factors for  $^{13}\text{C}$  nuclei of more than 2500. The method has interesting applications in MRI, especially in medicinal imaging and molecular spectroscopy.

The method yields unique mechanistic information, it permits the determination of kinetic parameters, it allows the determination of the degree of reversi-

bility of various homogeneous hydrogenations, it yields information about simultaneous (i.e., “pairwise” hydrogen transfer versus asynchronous transfer of individual hydrogens in subsequent events), and it also promises attractive applications to boost the normally low sensitivity of  $^1\text{H}$ -MRI and, in particular, of heteronuclear MRI.

By using PHIP-NMR studies, various intermediates such as the previously elusive dihydrides of neutral and cationic hydrogenation catalysts, as well as hydrogenation product/catalyst complexes, have already been detected during the hydrogenation of styrene derivatives using cationic Rh catalysts. Information about the substituent effect on chemical shifts and kinetic constants has been obtained via time-resolved PASADENA NMR spectroscopy (DYPAS).

### Acknowledgment

The financial support of the Deutsche Forschungsgemeinschaft (DFG), Bonn, Germany, and of the Fonds der Chemischen Industrie, Frankfurt/M., Germany, is gratefully acknowledged.

### Abbreviations

ALTADENA	Adiabatic Longitudinal Transport After Dissociation Engenders Net Alignment
CIDNP	chemically induced dynamic nuclear polarization
DFT	density functional theory
MRI	magnetic resonance imaging
NOE	nuclear Overhauser effect
ODIP	orthodeuterium-induced polarization
PART	parahydrogen-aided resonance transfer
PASADENA	Parahydrogen And Synthesis Allow Dramatically Enhanced Nuclear Alignment
PHIP	Para-Hydrogen Induced Polarization
SE	signal enhancement
SNR	signal-to-noise ratio

## References

- 1 Moser, W. R., Reaction Monitoring by High-Pressure Cylindrical Internal-Reflectance and Optical-Fiber Coupled Reactors. In: Moser, W. R., Slocum, D. W. (Eds.), *Homogeneous Transition Metal-Catalyzed Reactions*, American Chemical Society, Washington DC, 1992, Advanced Chemistry Series 230, p. 5.
- 2 Whyman, R., *In Situ Spectroscopic Studies in Homogeneous Catalysis*. In: Moser, W. R., Slocum, D. W. (Eds.), *Homogeneous Transition Metal-Catalyzed Reactions*, American Chemical Society, Washington DC, 1992, Advanced Chemistry Series 230, p. 19 and references therein.
- 3 (a) Roe, D. C., *Adv. Chem. Ser.* **1992**, 230, 33; (b) Elsevier, C. J., *J. Mol. Catal.* **1994**, 92, 258.
- 4 (a) Rathke, J. W., Klingler, R. J., Chen, M. J., Woelk, K., *Trends Organomet. Chem.* **1994**, 1, 117; (b) Woelk, K., Bargon, J., *Rev. Sci. Instrum.* **1992**, 63, 33070; (c) Trautner, P., Woelk, K., Bargon, J., et al., *J. Magn. Reson.* **2001**, 151, 284; (d) Niessen, H. P., Trautner, P., Wiemann, S., Bargon, J., Woelk, K., *Rev. Sci. Instr.* **2002**, 73 Part 1, 1259.
- 5 (a) Bryndza, H. E., Thesis, Berkeley, 1981; (b) Seidler, P. F., Bryndza, H. E., Frommer, J. E., Stuhl, L. S., Bergman, R. G., *Organometallics* **1983**, 2, 1701.
- 6 (a) Bowers, C. R., Weitekamp, D. P., *Phys. Rev. Lett.* **1986**, 57, 2645; (b) Bowers, C. R., Weitekamp, D. P., *J. Am. Chem. Soc.* **1987**, 109, 5541.
- 7 Eisenschmid, T. C., Kirrs, R. U., Deutsch, P. P., Hommeltoft, S. I., Eisenberg, R., Bargon, J., Lawler, R. G., Balch, A. L., *J. Am. Chem. Soc.* **1987**, 109, 8089.
- 8 (a) Barkemeyer, J., Haake, M., Bargon, J., *J. Am. Chem. Soc.* **1995**, 117, 2927; (b) Haake, M., Natterer, J., Bargon, J., *J. Am. Chem. Soc.* **1996**, 118, 8688, and references therein.
- 9 Pravica, M. G., Weitekamp, D. P., *Chem. Phys. Lett.* **1988**, 145, 255.
- 10 (a) Sandler, Y. L., *J. Phys. Chem.* **1954**, 58, 54–57; (b) Sandler, Y. L., *J. Chem. Phys.* **1958**, 29, 97.
- 11 Depatie, D. A., Mills, R. L., *Rev. Sci. Instr.* **1968**, 39, 105.
- 12 (a) Bowers, C. R., Jones, D. H., Kurur, N. D., Labinger, J. A., Pravica, M. G., Weitekamp, D. P., *Adv. Mag. Res.* **1990**, 14, 269; (b) Eisenberg, R., *Acc. Chem. Res.* **1991**, 24, 110; (c) Bargon, J., Kandels, J., Woelk, K., *Z. Phys. Chem.* **1993**, 180, 65.
- 13 Greve, T., Bargon, J., unpublished results.
- 14 Bargon, J., Kandels, J., Kating, P., *J. Chem. Phys.* **1993**, 98, 6150.
- 15 Kaptein, R., *J. Chem. Soc. Chem. Commun.* **1972**, 872.
- 16 (a) Lepley, A. R., Closs, G. L., *Chemically Induced Magnetic Polarization*, J. Wiley and Sons, New York, 1973; (b) Pine, S. H., *J. Chem. Edu.* **1972**, 49, 664, and references therein; (c) Carey, F. A., Sundberg, R. J., *Advanced Organic Chemistry*, Plenum Press, New York, 1984, 2nd edn, Part A, p. 623; (d) Buchachenko, A. L., Frankevich, E. F., *Chemical Generation and Reception of Radio- and Microwaves*, VCH Publishers, New York, 1994, p. 33; (e) Sweany, R. L., Halpern, J., *J. Am. Chem. Soc.* **1977**, 99, 8335.
- 17 Bargon, J., Kandels, J., Woelk, K., *Angew. Chem. Int. Ed.* **1990**, 29, 58; *Angew. Chemie* **1990**, 102, 70.
- 18 Bonhoeffer, K. F., Harteck, P., *Z. Phys. Chem.* **1929**, B4, 113.
- 19 (a) Sandler, Y. S., *J. Phys. Chem.* **1954**, 58, 58; (b) Sandler, Y. S., *J. Chem. Phys.* **1958**, 29, 97.
- 20 (a) Steinfeld, J. I., *Molecules and Radiation*, The MIT Press, Cambridge, Massachusetts, London, Third Printing, 1981, p. 98; (b) Sidgwick, N. V., *The Chemical Elements and Their Compounds*, Vol. I, Oxford University Press, Oxford, 1951; (c) Driesen, A., van der Poll, E., Silvera, I. F., *Phys. Rev.* **1984**, B30, 2317.
- 21 Buntkowsky, G., Bargon, J., Limbach, H. H., *J. Am. Chem. Soc.* **1996**, 118, 8677.
- 22 (a) Young, J. F., Osborn, J. A., Jardine, F. H., Wilkinson, G., *J. Chem. Soc., Chem. Commun.* **1965**, 131; (b) Osborn, J. A., Jardine, F. H., Young, J. F., Wilkinson, G., *J. Chem. Soc. A* **1966**, 1711
- 23 Tolman, C. A., Meakin, P. Z., Lindner, D. L., Jesson, J. P., *J. Am. Chem. Soc.* **1974**, 96, 2762.

- 24 Duckett, S. B., Newell, C. L., Eisenberg, R., *J. Am. Chem. Soc.* **1994**, *116*, 10548.
- 25 (a) Halpern, J., Okamoto, T., Zakhariev, A., *J. Mol. Catal.* **1976**, *2*, 65; (b) Dawans, F., Morel, D., *J. Mol. Catal.* **1977–78**, *3*, 403.
- 26 Schrock, R. R., Osborn, J. A., *J. Am. Chem. Soc.* **1976**, *98*, 2134.
- 27 (a) Halpern, J., Riley, D. P., Chan, A. S. C., Pluth, J. J., *J. Am. Chem. Soc.* **1977**, *99*, 8055; (b) Chan, A. S. C., Halpern, J., *J. Am. Chem. Soc.* **1980**, *102*, 838; (c) Halpern, J., *Inorg. Chim. Acta.* **1981**, *50*, 11; (d) Halpern, J., *Science* **1982**, *217*, 401; (e) Collman, J. P., Hegedus, L. S., Norton, J. R., Finke, R. G., *Principles and Applications of Organotransition Metal Chemistry*, University Science Books, Mill Valley, California, **1987**, p. 529.
- 28 Greve, T., PhD Thesis, Faculty of Sciences/Physics, University of Bonn, **1996**.
- 29 Duckett, S. B., Eisenberg, R., Goldman, A. S., *J. Chem. Soc., Chem. Commun.* **1993**, 1185.
- 30 Duckett, S. B., Eisenberg, R., *J. Am. Chem. Soc.* **1993**, *115*, 5292.
- 31 D., Colebrooke, S. A., Duckett, S. B., Lohman, J. A. B., Eisenberg, R., *J. Chem. Soc., Dalton Trans.* **1998**, 3363.
- 32 Esteruelas, M. A., Lahuerta, O., Modrego, J., Nürnberg, O., Oro, L. A., Rodriguez, L., Sola, E., Werner, H., *Organometallics* **1993**, *12*, 266.
- 33 (a) Dang, T. P., Kagan, H. B., *Chem. Commun.* **1971**, 481; (b) Knowles, W. S., Sackbacky, M. J., Vineyard, B. D., *Chem. Commun.* **1972**, 10.
- 34 (a) Harthun, A., Selke, R., Bargon, J., *Angew. Chem. Int. Ed.* **1996**, *35*, 2505; (b) Harthun, A., Barkemeyer, J., Selke, R., Bargon, J., *Tetrahedron Lett.* **1995**, *36*, 7423; (c) Natterer, J., Bargon, J., *Progr. NMR Spectr.* **1997**, *31*, 293; (d) Duckett, S. B., Sleigh, C. J., *Prog. NMR Spect.* **1999**, *34*, 71.
- 35 (a) Heinrich, H., Giernoth, R., Bargon, J., Brown, J. M., *Chem. Commun.* **2001**, 1296; (b) Giernoth, R., Heinrich, H., Adams, N. J., Bargon, J., Brown, J. M., *J. Am. Chem. Soc.* **2000**, *122*, 12381; (c) Giernoth, R., Hydrogenation. In: *Mechanisms in Homogeneous Catalysis: A Spectroscopic Approach*, B. Heaton (Ed.), John Wiley & Sons Inc., **2005**, p. 359.
- 36 (a) Landis, C. R., Feldgus, S., *Angew. Chem. Int. Ed.* **2000**, *39*, 2863; (b) Landis, C. R., Hilfenhaus, P., Feldgus, S., *J. Am. Chem. Soc.* **1999**, *121*, 8741; (c) Kless, A., Börner, A., Heller, D., Selke, R., *Organometallics* **1997**, *16*, 2096; (d) Bray, M. R., Deeth, R. J., Paget, V. J., Sheen, P. D., *Int. J. Quant. Chem.* **1997**, *61*, 85.
- 37 Giernoth, R., Hübler, P., Bargon, J., *Angew. Chem. Int. Edit.* **1998**, *37*, 2473.
- 38 Eichhorn, A., Koch, A., Bargon, J., *J. Mol. Catal. A – Chem.* **2001**, *174*, 293.
- 39 Bowers, C. R., Jones, D. H., Kurur, N. D., Labinger, J. A., Pravica, M. G., Weitekamp, D. P., *Adv. Magn. Reson.* **1990**, *14*, 269 and references therein.
- 40 Eisenberg, R., Eisenschmid, T. C., Chinn, M. S., Kirss, R. U., *Homogenous Transition Metal Catalyzed Reactions*. Moser, W. R., Slocum, D. W. (Eds.), *Advances in Chemistry* 230, Washington DC, **1992**, p. 45 and references therein.
- 41 Duckett, S. B., Newell, C. L., Eisenberg, R., *J. Am. Chem. Soc.* **1993**, *111*, 1156.
- 42 Stephan, M., Kohlmann, O., Niessen, H. G., Eichhorn, A., Bargon, J., *Magn. Reson. Chem.* **2002**, *40*, 157.
- 43 Aldrich/ACD Library of FT NMR Spectra Pro, V 1.7, **1998**.
- 44 Wildschütz, S., Hübler, P., Bargon, J., *Chem. Phys. Chem.* **2001**, *2*, 328.
- 45 (a) Schmidt, T., Bargon, J., unpublished results; (b) Schmidt, T., PhD Thesis, Bonn University, **2003**, [http://hss.ulb.uni-bonn.de/diss\\_online/math\\_nat\\_fak/2003/schmidt\\_thorsten/index.htm](http://hss.ulb.uni-bonn.de/diss_online/math_nat_fak/2003/schmidt_thorsten/index.htm).
- 46 (a) Limbacher, A., Jonischkeit, T., Bargon, J., to be published; (b) Limbacher, A., PhD Thesis, Bonn University, **2004**, [http://hss.ulb.uni-bonn.de/diss\\_online/math\\_nat\\_fak/2004/limbacher\\_arndt/index.htm](http://hss.ulb.uni-bonn.de/diss_online/math_nat_fak/2004/limbacher_arndt/index.htm); (c) Jonischkeit, T., PhD Thesis, Bonn University, **2004**, [http://hss.ulb.uni-bonn.de/diss\\_online/math\\_nat\\_fak/2004/jonischkeit\\_thorsten/index.htm](http://hss.ulb.uni-bonn.de/diss_online/math_nat_fak/2004/jonischkeit_thorsten/index.htm).
- 47 (a) Niessen, H. G., Schleyer, D., Wiemann, S., Bargon, J., et al., *Magn. Reson. Chem.* **2000**, *38*, 747; (b) Schleyer, D., Niessen, H. G., Bargon, J., *New. J. Chem.*

- 2001, 25, 423; (c) Schleyer, D., PhD Thesis, Bonn University, 2000. [http://hss.ulb.uni-bonn.de/diss\\_online/math\\_nat\\_fak/2000/schleyer\\_dana/index.htm](http://hss.ulb.uni-bonn.de/diss_online/math_nat_fak/2000/schleyer_dana/index.htm).
- 48 (a) Kuhn, L. T., Fligg, R., Bargon, J., unpublished results; (b) Kuhn, L. T., Bommerich, U., Bargon, J., submitted; (c) Bommerich, U., PhD Thesis, Bonn University, 2005. [http://hss.ulb.uni-bonn.de/diss\\_online/math\\_nat\\_fak/2005/bommerich\\_ute/index.htm](http://hss.ulb.uni-bonn.de/diss_online/math_nat_fak/2005/bommerich_ute/index.htm).
- 49 (a) Golman, K., Axelsson, O., Jóhannesson, H., Månsson, S., Olofsson, C., Petersson, J.S., *Magn. Reson. Med.* **2001**, 46, 1; (b) Golman, K., Ardenkjær-Larsen, J. H., Svensson, J., Axelsson, O., Hansson, G., Hansson, L., Jóhannesson, H., Leunbach, I., Månsson, S., Petersson, J.S., et al., *Acad. Radiol.* **2002**, 9 (Suppl. 2), S507; (c) Ardenkjær-Larsen, J. H., Fridlund, B., Gram, A., Hansson, G., Hansson, L., Lerche, M. H., Servin, R., Thaning, M., Golman, K., *Proc. Natl. Acad. Sci. USA* **2003**, 100, 10158; (d) Månsson, S., Johansson, E., Magnusson, P., Chai, C. M., Hansson, G., Petersson, J. S., Stahlberg, F., Golman, K., *Eur. Radiol.* **2005**, June 14 [Epub ahead of print]. [http://www.ncbi.nlm.nih.gov/entrez/query.fcgi?cmd=Retrieve&db=PubMed&list\\_uids=15954020&dopt=Citation](http://www.ncbi.nlm.nih.gov/entrez/query.fcgi?cmd=Retrieve&db=PubMed&list_uids=15954020&dopt=Citation) (November 15, 2005).
- 50 Bargon, J., to be published.
- 51 Koch, A., Bargon, J., *Magn. Reson. Chem.* **2000**, 38, 216.
- 52 Fligg, R., Bargon, J., Enrichment of parahydrogen using the Oxford closed cycle cooler cryostat. *Research Matters*, **2000**, 12, Oxford Instruments, Oxford, UK.
- 53 (a) Evett, A. A., *J. Chem. Phys.* **1959**, 31, 565; (b) White, D., Lassetre, E. N., *J. Chem. Phys.* **1960**, 32, 72; (c) Freeman, M. P., Hagyard, M. J., *J. Chem. Phys.* **1969**, 49, 4020.
- 54 Cunningham, C. M., Chapin, D. S., Johnston, H. L., *J. Am. Chem. Soc.* **1958**, 80, 2382.
- 55 Dosiere, M., *J. Chem. Edu.* **1985**, 62, 891.
- 56 Grilly, E. R., *Rev. Sci. Instrum.* **1953**, 24, 72.
- 57 Bradshaw, T. W., Norris, J. O. W., *Rev. Sci. Instr.* **1987**, 58, 83.
- 58 Koch, A., Bargon, J., *Inorg. Chem.* **2001**, 40, 533.
- 59 Carson, P. J., Bowers, C. R., Weitekamp, D. P., *J. Am. Chem. Soc.* **2001**, 123, 11821.
- 60 Sulman, E., Deibele, C., Bargon, J., *React. Kinet. Catal.* **1999**, L67 (1), 117.
- 61 Jang, M., Duckett, S. B., Eisenberg, R., *Organometallics* **1996**, 15, 2863.
- 62 Duckett, S. B., Mawby, R. J., Partridge, M. G., *Chem. Commun.* **1996**, 383.
- 63 Millar, S. P., Zubris, D. L., Bercaw, J. E., Eisenberg, R., *J. Am. Chem. Soc.* **1998**, 120, 5329.
- 64 Suardi, G., Cleary, B. P., Duckett, S. B., Sleigh, C., Rau, M., Reed, E. W., Lohman, J. A. B., Eisenberg, R., *J. Am. Chem. Soc.* **1997**, 119, 7716.
- 65 Bowers, C. R., Sensitivity enhancement utilizing parahydrogen. In: Grant, D. M., Harris, R. K. (Eds.), *Encyclopedia of Nuclear Magnetic Resonance*, Volume 9, **2002**, p. 1.